Eur. Phys. J. C (2024) 84:54
https://doi.org/10.1140/epjc/s10052-024-12402-8

THE EUROPEAN PHYSICAL JOURNAL C

Check for updates

Regular Article - Theoretical Physics

A possible critical heating from decay reaction and new upper limit of the magnetic monopole flux for the supermassive white dwarfs

Jing-Jing Liu[a], **Dong-Mei Liu**

College of Science, Hainan Tropical Ocean University, Sanya 572022, China

Received: 7 October 2023 / Accepted: 4 January 2024
© The Author(s) 2024

Abstract We present the new upper limit of the magnetic monopole (MM) flux and discuss three MM models of the heating resource for supermassive white dwarfs (WDs) by considering the effect of temperature on thermonuclear reaction and mass radius relation of WDs based on the catalytic nuclear decay by MM. We discuss the luminosity and compared it with the observations to apply to 25 supermassive WDs. We find the maxnium of the number of MM captured can be 9.6943×10^{11}, and 9.0671×10^{11} for O+Ne core high mass WDs (e.g., WD J055631.17+130639.78), and C+O core high mass WDs (e.g., WD J055631.17+130639.78), respectively. The luminosities increase with the increasing of the temperature and are agreed well with the observations for model (III). The differences are no more than one, and three orders of magnitude higher than observations for model (III), and (I, II), respectively. Finaly, we find that the maxnium of the upper limits of the MM flux ϕ_m due to RC effect can be 9.1071×10^{-15}, and 2.7670×10^{-14} for O+Ne and C+O core high mass WDs, respectively. Our results are about one and two orders of magnitude higher than those of Abbasi et al. (EPJC 69:361, 2010) (Albert et al. in JHEP 07:054, 2017) for O+Ne, and C+O core mass WDs, respectively, and can be about three and four orders of magnitude higher than those of Aartsen et al. (EPJC 76:133, 2016) (Ic40, Ic86), respectively. Our results show that the monopole-catalyzed nucleon decay could prevent WDs from cooling down into a stellar graveyard by keeping them hot.

1 Introduction

White dwarfs (hereafter WDs) are usually made up of C+O. It is also possible that the core will be hot enough to burn carbon but not hot enough to burn Ne, and then a WDs with a core of O+Ne+Mg will form. There is no matter inside the WDs to undergo nuclear fusion, so the star can no longer produce energy. It is no longer protected by the heat of fusion against gravitational collapse, but is supported by the electron degeneracy pressure of extremely dense matter. As the mass grows further, the electron degeneracy pressure may fail to resist its own gravitational contraction, and the WDs may collapse into even denser objects at very high temperatures.

Because they have no source of energy, it will therefore gradually give off its heat and gradually cool by dropping its temperature, which means that its radiation will decrease over time from its initial high color temperature to turn red. This surface temperature is defined in astronomy as the effective temperature $T_{\rm eff}$ by means of Stefan's law, so that

$$L_{\rm rad} = 4\pi R^2 \sigma T_{\rm eff}^4, \tag{1}$$

where R the radius of the star, and $L_{\rm rad}$ is the radiation luminosity, and and $\sigma = 5.6704 \times 10^{-5}\,{\rm ergs}^{-1}\,{\rm cm}^{-2}\,{\rm K}^{-4}$ is the radiation constant from Stefan's law. The $T_{\rm eff}$ is a measure of the energy flux at the surface and not a real temperature, but it nevertheless constitutes a useful measure of the atmospheric temperature of the star.

The radius of a WDs is about $\sim 10^4$ Km, the surface temperature is about $5 \times 10^3 \sim 4 \times 10^4$ K. The internal temperature of a WDs is about $\sim 10^6 - 10^7$ K, and the total thermal energy is less than 10^{47} ergs. The effective temperature of WDs is mostly from 5500 to 40,000 K, and a few WDS can be outside this range. According to Eq. (1), the radiation luminosity of a WD is about $\sim 10^{31}$ ergs/s. Therefore, its typical cooling time is marked as $t_{\rm cool} \approx 10^{16} s \approx 3.3 \times 10^8$ years. In other words, the WDs should cool down in $(1 \sim 10)$ billion years.

According to some observations, the colors of the WDs can be from O to K types, and some WDs have the colors of the M-type. Why do most WDs have spectral types above A (such as O, B, and A type), a few WDs are F, G, and K-type, and there are few late M and N type WDs with

[a] e-mail: liujingjing68@126.com (corresponding author)

Published online: 18 January 2024

the surface temperature below 3000 K? What are their specific heat sources, which can provide this energy? These are extremely interesting issues to study.

References [1,2] discussed the energy sources of WDs. Reference [3] also studied the configurations of hot WDs with nuclear sources of energy. They suggested that there are small amounts of ^{22}Ne in some WDs, which may be an extra source of heat in carbon-oxygen WDs. The single-particle ^{22}Ne sedimentation may be considered a possible heat source [4,5]. However, some works suggest that ^{22}Ne must separate into clusters, enhancing diffusion, in order for sedimentation to provide heating on the observed timescale. Recently, the sources of ultra-high energetic photons for the WD pulsars have been discussed by Ref. [6]. Reference [7] discussed the cooling anomaly of high-mass WDs. They pointed out that ^{22}Ne settling in C/O-core WDs could account for this extra cooling delay. Reference [8] studied this topic using molecular dynamics methods and phase diagrams. They ruled out the isotope of ^{22}Ne as a possible cause of the extra heating. Therefore, the problem of additional heat source for WDs remains a challenging topic.

Some studies (e.g., [9,10]) shown that the magnetic monopoles (hereafter MMs) catalytic nuclear decay (RC effect) [11,12] may be very important in the cooling of WDs. MM is a hypothetical magnetic particle with a single magnetic pole at the north or South Pole. The research of MMs has always been a forefront subject of physicists and astronomers. Some papers discussed the issue about MMs, (e.g., [13–18]). Recently, we are interesting in the problem of MMs and other related issues (e.g., [19–25]). Some scholars also discussed other energy mechanisms of WDs, and neutron star, such as magnetic field evolution, and related issues (e.g., [26–29]). In this paper, we select 25 typical supermassive WDs [30], and present three models to solve the energy source problem based on the RC effect [11,12].

2 The magnetic monopoles and the numbers captured by Star in space

According to some researches by physicists, the interaction of MMs with neutral hydrogen atoms is very weak. During the process of the formation of heavenly bodies, very few MMs follow the collapse of a neutral hydrogen cloud and assemble in the core of a star or planet. The MMs usually may be contained inside stars and planets, and they are mostly captured from the universe in their lifetime after their formation.

The total number of MMs captured in space after the formation of stars (or planets) is [9,10,31–34]

$$N_m = 4\pi^2 R^2 \eta \phi_m t \left[1 + \frac{v_{\rm esc}^2}{v_m^2}\right], \tag{2}$$

where $v_{\rm esc} = (2GM/R)^{1/2}$ is the escape velocity from the star, and t is the lifetime for the star. For the planet, $\frac{v_{\rm esc}^2}{v_m} \ll 1$, and $\frac{v_{\rm esc}^2}{v_m} \approx 1$ for ordinary stars, but $\frac{v_{\rm esc}^2}{v_m} \gg 1$ for compact object, such as WDs, neutron star, Galactic nuclei and quasars. The velocity v_m of the MMs in space is given by [35]

$$v_m \approx \begin{cases} 3.0\times 10^{-3} c(10^{16}\,{\rm GeV}/m)^{1/2} & (m < 10^{17}\,{\rm GeV}) \\ 10^{-3}c & ({\rm otherwise}). \end{cases} \tag{3}$$

The ratio between the number of MMs captured and the number of nuclei in the MMs accumulation area is [24,25,33]

$$\begin{aligned} \zeta_m^{\rm cap} &= \frac{N_m^{\rm cap}}{N_{\rm B}} = 5.1\times 10^{-34}\eta\left[1 + 10^6\left(\frac{10^{-3}c}{v_m}\right)^2\left(\frac{R_g}{R}\right)\right] \\ &\quad\times\left(\frac{R}{R_\odot}\right)^2\left(\frac{M_\odot}{M}\right)\left(\frac{\phi_m}{\phi_0}\right)\left(\frac{t}{10^9 yr}\right) \\ &= 5.1\times 10^{-34}\eta R_*^2\left(\frac{t_9}{M_*}\right)\left(\frac{\phi_m}{\phi_0}\right) \\ &\quad\times\left[1 + 10^6\left(\frac{10^{-3}}{\beta}\right)^2\left(\frac{R_g}{R}\right)\right] \\ &= 5.1\times 10^{-34}\eta R_*^2\left(\frac{t_9}{M_*}\right)\left(\frac{\phi_m}{\phi_0}\right)\left[1 + 4.256 v_{-3}^{-2}\left(\frac{M_*}{R_*}\right)\right], \end{aligned} \tag{4}$$

where R, t are the radius and the age of the star, respectively. $R_* = R/R_\odot$, $M_* = M/M_\odot$, and $t_9 = t/10^9$yr is the cooling time. $\beta = v_m/c$, $v_{-3} = \beta/10^{-3}$, and $R_g = 2.96\times 10^5 M_*$ is the Schwarzschild radius. $M_\odot = 1.99\times 10^{33}$ g, $R_\odot = 6.955\times 10^{10}$ cm are the mass and the radius of the sun, respectively. ϕ_m is the flux of MMs intercepted in space, and $\phi_0 \approx 10^{-16}{\rm cm}^{-2}\,{\rm s}^{-1}\,{\rm Sr}^{-1}$ is the upper limit of the flux of MMs of Parker [36]. Then it is modified to be $\phi_0 \approx 10^{-12}{\rm cm}^{-2}\,{\rm s}^{-1}\,{\rm Sr}^{-1}$ by [37]. η is the probability captured of MMs by stars, which is depended on the ratio of the penetration distance l_{pd} of a MM in a star to the radius of the star.

In general, we have $l_{pd} \approx 1.2\times 10^{30} v_{-3} n_e^{-1} T_e^{1/2}$ for plasma. For example, $n_e \sim 10^{22}\,{\rm cm}^{-3}$, $T_e \sim 10^6$ K, for sun, we have $l_{pd} \sim 10^{11}$, $\eta \sim 0.7$. However, $n_e > 10^{30}\,{\rm cm}^{-3}$, and $n_e > 10^{35}\,{\rm cm}^{-3}$ for WDs and neutron star, respectively, we have $\eta \sim 1$. For quasars and active galactic nuclei, $M \sim 10^8 M_\odot$, $R/R_g \sim 10$, and $T_e \sim 10^5$ K, we also have $\eta \sim 1$ (e.g., [33]). The number density of nucleons can be written by [33]

$$\begin{aligned} n_B &= 2.90\times 10^{16}\left(\frac{R}{R_g}\right)^{-3}(M_{12})^{-2} \\ &= 2.236\times 10^{24}\left(\frac{M}{M_\odot}\right)\left(\frac{R}{R_\odot}\right)^{-3} \\ &= 2.236\times 10^{24} M_* R_*^{-3}\,{\rm cm}^{-3}, \end{aligned} \tag{5}$$

where $M_{12} = M/(10^{12} M_\odot)$.

For WDs, in Eq. (4) we take $\phi_0 \approx 10^{-12}\text{cm}^{-2}\ \text{s}^{-1}\ \text{Sr}^{-1}$ [37], $\eta \sim 1$ and $4.256 v_{-3}^{-2}(\frac{M_*}{R_*}) \gg 1$. According to Eqs. (4) and (5), the total number of MMs captured by WDs is

$$\begin{aligned} N_{m(\text{tot})} &= 7.1834 \times 10^{16} n_B \phi_m R_*^5 \left(\frac{t_9}{M_*}\right) \\ &\quad \times \left[1 + 4.256 v_{-3}^{-2}\left(\frac{M_*}{R_*}\right)\right], \\ &\approx 6.83597 \times 10^{41} \phi_m t_9 M_* R_* v_{-3}^{-2}. \end{aligned} \tag{6}$$

3 The luminosity function due to catalytic nuclear decay (RC effect)

The MM catalyze nuclear decay reaction (hereafter RC effect) can be expressed by $pM \to e^+\pi^0 M + \text{debris}(85\%)$, and $pM \to e^+\mu^\pm M + \text{debris}(15\%)$ [11,12]. The reaction cross section is about $\sigma_m \approx 10^{-25} \sim 10^{-26}\,\text{cm}^2$, almost reaching the Thomson cross section ($6.665 \times 10^{-25}\,\text{cm}^2$).

The luminosity due to the RC effect of various types of celestial bodies (i.e., RC luminosity) can be estimated as follows. In the core area, where the MM is concentrated, the nuclear decay reaction is catalyzed by the MMs and the total luminosity produced is [33]

$$L_m \approx \frac{4\pi}{3} r_c^3 n_m n_\text{B} \langle \sigma_m v_\text{T} \rangle m_\text{B} c^2 = N_m n_B \langle \sigma_m v_\text{T} \rangle m_\text{B} c^2, \tag{7}$$

where r_c, and n_m, n_B are the radius of the stellar central region, the number density of MMs and nucleons, respectively.

We ignore the number of MMs deposited into the core of the star as the neutral hydrogen (nebula) cloud collapses during the formation of stars and planets. This is because the neutral hydrogen cloud interacts very weakly with the MM. During the collapse process, a very small number of MMs gather at the center of the star as the nebula collapses.

In Eq. (7), σ_m is the reaction cross section of the RC effect. As a general rule, it is from $10^{-26} \sim 10^{-24}\,\text{cm}^2$. v_T is the thermal movement speed of the nucleus relative to the MM. We will ignore thermal motion velocity of the MM due to it is too heavy. So we only consider the contributions from the thermal motion velocity of the nucleus. According to $1/2 m v_T^2 = 3/2 kT$, we have

$$v_\text{T} = \sqrt{3kT/m_B} \approx 1.5745 \times 10^7 T_6^{1/2}\ \text{cm/s}, \tag{8}$$

where T is the temperature, $T_6 = T/10^6$ K and $k = 1.38 \times 10^{-16}$ erg/s is the Boltzmann constant, $m_B \approx 1.67 \times 10^{-24}$g is the nucleons mass. When the center temperature of the WDs is about $\sim 10^6$ K, we have $v_T \sim 10^{-3} c$.

In the RC process MMs induced nucleon decay, followed by nucleon decay into π^0 meson, $\mu^\pm$ leptons and proton e^+. Then $\mu^\pm$ and π^0 again decay into photons rand election proton pairs $e^\pm$. The protons finally annihilate with the electrons to photons. The net effect is that the rest mass energy of nucleons ($m_\text{B} c^2$) entirely converted to radiation energy with 100% efficiency.($1 m_\text{B} c^2 \approx 1\text{GeV} \approx 1.6 \times 10^{-3}$ erg).

4 The magnetic monopole model and RC luminosity inside white dwarfs

4.1 The magnetic monopole model (I) in WDs

4.1.1 The classic mass–radius relation in WDs

Through functions of two dimensionless variables $\eta = U/kT$ and $\vartheta = kT/m_e c^2$ (where m_e is the mass of the electron, and U the chemical potential), the equation of the state for electron gas in WDs can be derived from the distribution function in parameterized form and given by [38]

$$P = \frac{16\pi\sqrt{2}}{3} \frac{m_e^4 c^5}{h^2} \vartheta^{5/2} [F_{3/2}(\eta, \vartheta) + (\vartheta/2) F_{5/2}(\eta, \vartheta)], \tag{9}$$

$$n_e = 8\pi\sqrt{2} \frac{m_e^3 c^3}{h^3} \vartheta^{3/2} [F_{1/2}(\eta, \vartheta) + \vartheta F_{3/2}(\eta, \vartheta)], \tag{10}$$

$$\varepsilon = 8\pi\sqrt{2} \frac{m_e^4 c^5}{h^3} \vartheta^{5/2} [F_{3/2}(\eta, \vartheta) + \vartheta F_{5/2}(\eta, \vartheta)], \tag{11}$$

where

$$F_n(\eta, \vartheta) = \int_0^\infty \frac{x^n (1 + x\vartheta/2)^{1/2} dx}{\exp(\eta + x) + 1}, \tag{12}$$

where P, n_e and ε are the pressure, electron number density and energy density, respectively. In Eq. (12), $x = p_F/m_e c$, and $1 + x^2 = (1 + \eta\vartheta)^2$.

According to the discussions from [38], the electron number density and the pressure are written by

$$n_e = \frac{2}{h^3} \int_0^\infty 4\pi p^2 dp = \frac{8\pi m_e c^3}{3h^3} = \frac{8\pi m_e c^3}{3h^3} x^3 \tag{13}$$

$$P = \frac{8\pi}{3h^3} \int_0^\infty \frac{(p^4/m_e) dp}{\sqrt{1 + (p/m_e c)^2}}, \tag{14}$$

where

$$f(x) = x(x^2 + 1)^{1/2}(2x^2 - 3) + 3\ln(x + \sqrt{1 + x^2}) \tag{15}$$

The classical mass–radius relation of WDs is one of interesting issue for astrophysicist. For zero-temperature stars, the equations of hydrostatic equilibrium and of mass conservation are given by

$$\frac{dP}{dr} = -\frac{G m_r \rho}{r^2}, \tag{16}$$

$$\frac{dM}{dr} = 4\pi r^2 \rho, \tag{17}$$

where r is the radial variable (when $r = 0$ at the center) and m_r is the mass inside a sphere of radius r.

Reference [39] discussed the mass–radius relation and achieved following expression

$$R_*(\mathrm{I}) \approx \frac{P_0}{R_\odot G(\rho_0\mu_e)^{5/3}} M^{-1/3} = 1.080\times 10^{-2}\mu_e^{-5/3}M_*^{-1/3}, \quad (18)$$

where $P_0 = \pi m^4c^5/(3h^3) \approx 5.9637\times 10^{22}$, and $\mu_e = A/Z$ is the molecular weight per electron, $\rho_0 = n_0 u \approx 9.6838\times 10^5$, $n_0 = 8\pi m^3c^3/(3\,h^3) \approx 5.8336\times 10^{29}$, and u is atoms mass unit. According to Eqs. (5, 18), we have

$$n_B(\mathrm{I}) = 2.236\times 10^{24} M_*(R_*(\mathrm{I}))^{-3} = 1.7750\times 10^{30}\mu_e^5 M_*^2\ \mathrm{cm}^{-3}. \quad (19)$$

4.1.2 The magnetic monopole model (I) in WDs

Reference [10] discussed the bound on the flux of MMs from catalysis of nucleon decay in WDs [9,10]. In their work, based on some new observational data of the cooling WD 1136-286 with the luminosity $10^{-4.94}L_\odot$, they investigated the number of MMs captured by a WD. The energy of the MM will be lost when a MM passes through a WD and is captured. Electronic interactions are considered to be the primary source of energy loss for the MM, with $dE/dx = 100\rho v_m$ GeV/cm, where v_m is the velocity of a MM as it passes through the WDs [40]. The MMs captured by a WD is given by [9,10]

$$N_1 = N_m(\mathrm{I}) \approx \phi_m(\mathrm{I}) A\tau(\pi sr) \approx 2.0\times 10^{39} a_1\phi_m(\mathrm{I}) = 2.3183\times 10^{40} t_9 R_*(\mathrm{I}) M_* v_{-3}^{-2}\phi_m(\mathrm{I}), \quad (20)$$

where $A = 4\pi R^2(1+2GM/(Rv_m^2))$, and $v_{-3} = v_m/10^{-3}c$, A is the capture area, and $a_1 = 0.1 t_9 R_9 M_{0.6} v_{-3}^{-2}$, where $R_9 = R/10^9 = 69.55R/R_\odot = 69.55R_*(\mathrm{I})$, $M_{0.6} = M/0.6M_\odot = M_*/0.6$.

From catalyzed nucleon decay process in their model (we note model (I)), the luminosity per monopole can be written

$$L_0 = \rho_c\sigma_m v_\mathrm{T} = 8.1\times 10^7(\sigma_m v_\mathrm{T})_{-28} s_{-2} M_{0.6} R_9^{-3}. \quad (21)$$

The total luminosity of a WD due to RC effect is given by

$$L_m(\mathrm{I}) = N_m(\mathrm{FK})L_0 = N_1 L_0 = 1.6\times 10^{47} a_2\phi_m(\mathrm{I}) = 9.188\times 10^{42} M_*^2 R_*^{-2}(\mathrm{I})(\sigma_m v_\mathrm{T})_{-28} v_{-3}^{-2} t_9\phi_m(\mathrm{I})\ \mathrm{erg\ s}^{-1}, \quad (22)$$

where $a_2 = 0.1 t_9 M_{0.6}^2 R_9^{-2}(\sigma_m v_m)_{-28} s_{-2} v_{-3}^{-2}$, s_{-2} is the fact of suppression effects, which may reduce the cross section of RC effect [31]. For example, the suppression effects would be less effective ($s_{-2} \approx 10$) in helium WDs.

4.2 Magnetic monopole catalytic nuclear decay model (II) in WDs

4.2.1 The new mass–radius relation in WDs in model (II)

WDs are compact objects, formed at the final evolution stage of middle mass and low mass main sequence stars. How to understand the nature of the mass–radius relation in WDs? Many astronomers have become very interested in this subject (e.g., [41–45]).

Reference [46] investigated the highly accurate relation between the radius and mass of the WDs from zero to finite temperature. He estimated the temperature effect by using statistical mechanics and found the complicated form of the pressure depended on temperature at the given particle number and volume. According to his discussions, the mass–radius relation in WDs for relativistic condition can be written by [46]

$$R_*(\mathrm{II}) = \frac{M^{1/3}\left(\frac{9h^3}{64\pi^2 m_n}\right)^{1/3}}{m_e c R_\odot\left[1-\frac{2\pi^2}{3}\left(\frac{kT}{m_e c^2}\right)^2\right]^{1/2}}\left[1-\left(\frac{M}{M_0}\right)^{2/3}\right]^{1/2} = \frac{1.808 M_*^{1/3}\left(\frac{9h^3}{64\pi^2 m_n}\right)^{1/3}}{m_e c\left[1-\frac{2\pi^2}{3}\left(\frac{kT}{m_e c^2}\right)^2\right]^{1/2}}\left[1-\left(\frac{M_*}{1.44}\right)^{2/3}\right]^{1/2} = 8.9513\times 10^{-3}\frac{M_*^{1/3}\left[1-\left(\frac{M_*}{1.44}\right)^{2/3}\right]^{1/2}}{\left[1-\frac{2\pi^2}{3}\left(\frac{kT}{m_e c^2}\right)^2\right]^{1/2}}, \quad (23)$$

where $h = 6.626\times 10^{-27}$erg s, and $k = 1.38065\times 10^{-16}$erg/K is the Planck and Boltzmann constant, respectively. $M_0 = 1.44M_\odot$, and m_e, m_n are the mass of a electron and neutron, respectively. $1m_e c^2 = 0.511\mathrm{MeV} = 8.176\times 10^{-7}$erg.

4.2.2 Magnetic monopole catalytic nuclear decay model (II) in WDs

According to Eq. (6), in the case without considering the RC effect on the relation of mass–radius, we can estimate the number of MMs captured from space in the lifetime of the WDs predecessor star as

$$N_2 = N_{m(\mathrm{tot})}(\mathrm{II}) \approx 6.83597\times 10^{41}\phi_m(\mathrm{II}) t_9 M_* R_*(\mathrm{II}) v_{-3}^{-2}. \quad (24)$$

The number density of nucleons for model (II) can be written by

$$n_B(\mathrm{II}) = 2.236\times 10^{24} M_* R_*^{-3}(\mathrm{II})\ \mathrm{cm}^{-3}. \quad (25)$$

According to Eqs. (7, 23–25), the total luminosity due to the nuclear decay reaction catalyzed by the MMs is given by

$$\begin{aligned} L_m(\mathrm{II}) &\approx \frac{4\pi}{3} r_c^3 n_m n_{\mathrm{B}}(\mathrm{II}) \langle \sigma_m v_{\mathrm{T}} \rangle m_{\mathrm{B}} c^2 \\ &= N_2 n_B(\mathrm{II}) \langle \sigma_m v_{\mathrm{T}} \rangle m_{\mathrm{B}} c^2 \\ &= 1.52852 \times 10^{66} M_*^2 R_*^{-2}(\mathrm{II}) v_{-3}^{-2} \langle \sigma_m v_{\mathrm{T}} \rangle \phi_m(\mathrm{II}) t_9. \end{aligned} \tag{26}$$

4.3 Magnetic monopole catalytic nuclear decay model (III) in WDs

When WDs stars mass is annihilated to contribute to a stellar energy source, we can propose the basic equations describing stars. The basic equations are given by [47]

$$\frac{\partial^2 r}{\partial t^2} = -4\pi r^2 \frac{\partial P}{\partial M(\mathrm{r})} + F_{\mathrm{r}} + \frac{\partial r}{\partial t} \frac{\varepsilon_{\mathrm{m}}}{c^2}, \tag{27}$$

$$\begin{aligned} &\frac{\partial E_{\mathrm{I}}}{\partial t} + P \frac{\partial}{\partial t} \left(\frac{1}{\rho} \right) = -\frac{\partial L_{\mathrm{r}}}{M(\mathrm{r})} + \varepsilon_{\mathrm{extr}} + \varepsilon_{\mathrm{m}} \\ &\quad + \frac{P \varepsilon_{\mathrm{m}}}{\rho c^2} + \frac{\varepsilon_{\mathrm{m}}}{\rho c^2} \left(E_{\mathrm{I}} - \frac{v_{\mathrm{r}}^2}{2} \right), \end{aligned} \tag{28}$$

$$\frac{\partial^2 M(\mathrm{r})}{\partial t \partial r} = -4\pi r^2 \frac{\rho \varepsilon_{\mathrm{m}}}{c^2}, \tag{29}$$

$$F_{\mathrm{r}} = -\frac{G M(\mathrm{r})}{r^2}, \tag{30}$$

$$M(\mathrm{r}) = \int_0^r 4\pi r^2 \rho dr, \tag{31}$$

where ε_{m} is the energy generation rate per unit mass by mass annihilation. F_{r}, E_{I}, and $\varepsilon_{\mathrm{extr}}$ are external force acting per unit mass, the internal energy density, and the energy generation (or loss) rate per unit mass by other processes such as nuclear burning and neutrino loss, respectively.

By eliminating the terms which include $\partial/\partial t$ in Eqs. (27)–(31), we can investigate the structure of stars in a quasi-static gravitational equilibrium when only the Rubakov process is taken into account as an energy release process. We obtain

$$\frac{\partial P}{\partial M(\mathrm{r})} = -\frac{G M(\mathrm{r})}{4\pi r^4}, \tag{32}$$

$$\frac{\partial L_{\mathrm{r}}}{\partial M(\mathrm{r})} = \varepsilon_{\mathrm{m}}, \tag{33}$$

$$\frac{\partial M(\mathrm{r})}{\partial r} = 4\pi r^2 \rho, \tag{34}$$

According to Eqs. (32–34), the relation of the mass–radius due to the number of the MMs captured and RC effect for some low mass stars, and gave following expression (e.g., [47])

$$\begin{aligned} R_*(\mathrm{III}) &\approx 2 \times 10^{-10} \left(\frac{M}{M_\odot} \right)^{-2.35} N_3^{0.45} \\ &= 2 \times 10^{-10} M_*^{-2.35} N_3^{0.45}, \end{aligned} \tag{35}$$

According to Eq. (5, 35), we have

$$\begin{aligned} n_B(\mathrm{III}) &= 2.2236 \times 10^{25} M_* R_*^{-3}(\mathrm{III}) \\ &= 2.7790 \times 10^{54} N_3^{-1.35} M_*^{8.05}\ \mathrm{cm}^{-3}. \end{aligned} \tag{36}$$

By considering the RC effect on the relation of mass–radius, according to Eq. (5), the numbers of MMs captured from space in the lifetime of the WDfs are given as

$$N_3 = 1.36719 \times 10^{31} \phi_m(\mathrm{III}) t_9 M_*^{-1.35} N_3^{0.45} v_{-3}^{-2}, \tag{37}$$

So we obtain

$$N_3 = \exp \left[\frac{\ln(1.36719 \times 10^{31} \phi_m(\mathrm{III}) t_9 M_*^{-1.35} v_{-3}^{-2})}{0.55} \right]. \tag{38}$$

According to Eqs. (7, 36, 38), the total luminosity in model (III) is given by

$$\begin{aligned} L_m(\mathrm{III}) &\approx \frac{4\pi}{3} r_c^3 n_m n_{\mathrm{B}}(\mathrm{III}) \langle \sigma_m v_{\mathrm{T}} \rangle m_{\mathrm{B}} c^2 \\ &= N_3 n_B(\mathrm{III}) \langle \sigma_m v_{\mathrm{T}} \rangle m_{\mathrm{B}} c^2 \\ &= 4.4720 \times 10^{50} \langle \sigma_m v_{\mathrm{T}} \rangle N_3^{-0.35} M_*^{8.05}. \end{aligned} \tag{39}$$

5 Results and discussions

5.1 The number of the MMs captured

The study on the MMs has been considerable interest issue since MMs were discovered to be a generic feature of grand unified gauge theories in the astrophysical fields. The theoretical predictions for the monopole abundance are problematic in the standard cosmology, far too many monopoles survive annihilation for the universe to have reached its present state. For example, the galactic field yields the Parker bound is $\phi_m(\sigma_m v)_{-28} \leq 10^{-16}\,\mathrm{cm}^{-2}\,\mathrm{s}^{-1}\,\mathrm{sr}^{-1}$ [36]. If we select $v = 10^{-3}c$, $\sigma_m = 10^{-26}$, we can obtain $\phi_m \leq 3.33 \times 10^{-26}\,\mathrm{cm}^{-2}\,\mathrm{s}^{-1}\,\mathrm{sr}^{-1}$. Due to the MM RC decay in neutron stars, a limit on the product of the flux and the catalysis cross section may be $\phi_m(\sigma_m v)_{-28} \leq 10^{-21}\,\mathrm{cm}^{-2}\,\mathrm{s}^{-1}\,\mathrm{sr}^{-1}$ [37]. We can also obtain $\phi_m \leq 3.33 \times 10^{-31}\,\mathrm{cm}^{-2}\,\mathrm{s}^{-1}\,\mathrm{sr}^{-1}$. A better understood limit comes from catalysis in WDs may be $\phi_m(\sigma_m v)_{-28} \leq 10^{-18}\,\mathrm{cm}^{-2}\,\mathrm{s}^{-1}\,\mathrm{sr}^{-1}$ [9]. we can obtain $\phi_m \leq 3.33 \times 10^{-28}\,\mathrm{cm}^{-2}\,\mathrm{s}^{-1}\,\mathrm{sr}^{-1}$. From the observed X-ray luminosities of neutron stars, [47] have obtained a limit to the monopole flux in the Galaxy as $\phi_m \leq 10^{-24}\,\mathrm{cm}^{-2}\,\mathrm{s}^{-1}\,\mathrm{sr}^{-1}$. In the monopole-catalysed nucleon decay, [47] assumed the cross section to be as large as that of strong interactions (i.e. $\sigma_m \sim 10^{-26}\,\mathrm{cm}^3$). Then the bound on the flux of MMs due to RC effect in WDs was discussed by [10]. Their results shown that the bound has been stated as $\phi_m(\sigma_m v)_{-28} < 1.3 \times 10^{-20}(v/(10^{-3}c)^2)\,\mathrm{cm}^{-2}\,\mathrm{s}^{-1}\,\mathrm{sr}^{-1}$. we can obtain $\phi_m < 4.33 \times 10^{-30}\,\mathrm{cm}^{-2}\,\mathrm{s}^{-1}\,\mathrm{sr}^{-1}$.

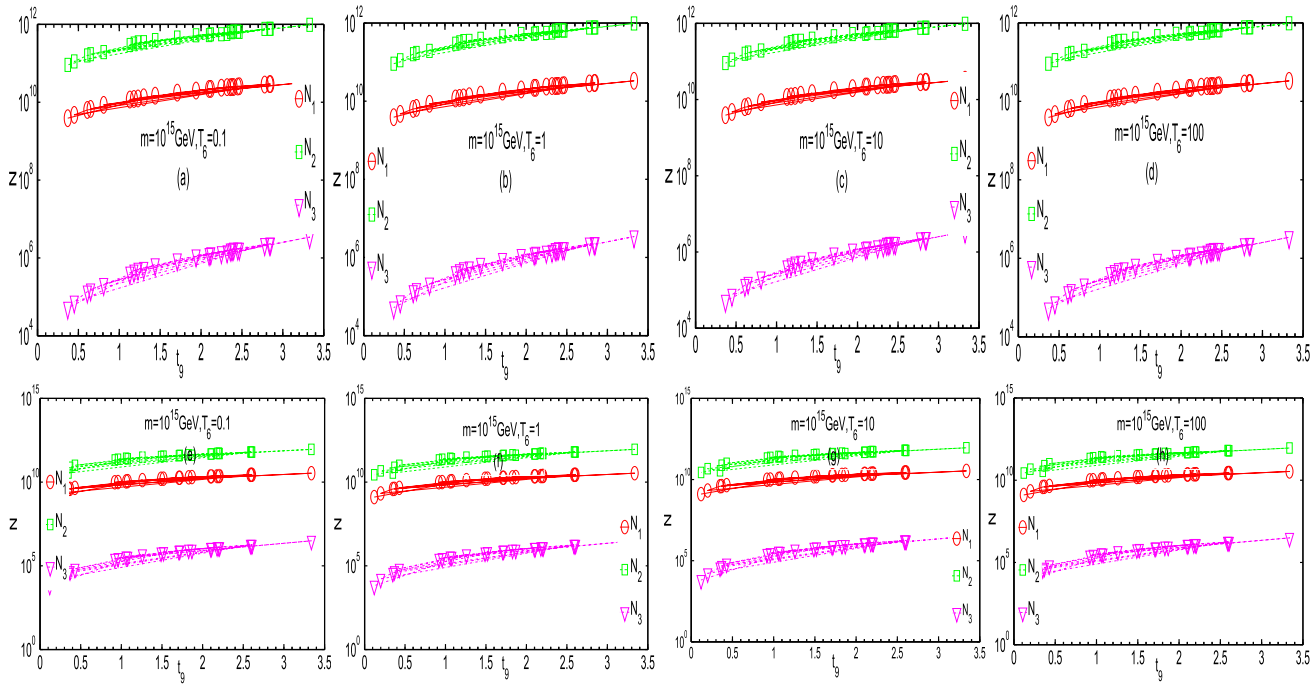

Fig. 1 The number of magnetic monopoles captured from space in the lifetime of the O+Ne (**a**–**d**) and C+O (**e**–**h**) core high mass WDs [30] for model (I, II, III) as a function of t_9 when $m = 10^{15}$ GeV, and $\sigma_m = 10^{-26}$ cm^2, $\phi_m = 10^{-26}$ cm^{-2} s^{-1} sr^{-1} at the temperature of $T_6 = 0.1, 1, 10, 100$

In this paper, we study the MMs and its numbers in space. We discuss our MM model and the luminosity function due to catalytic nuclear decay. We select some typical parameters as follows. The RC cross section, and the flux of MMs are selected by $\sigma_m = 10^{-26}\,\mathrm{cm}^2$, and $\phi_m = 10^{-26}$, $10^{-28}\,\mathrm{cm}^{-2}\,\mathrm{s}^{-1}\,\mathrm{sr}^{-1}$, respectively. Some typical temperatures and the mass of a MM are also selected by $T_6 = 0.1, 1, 10, 100$, and $m = 10^{15}$, 10^{18} GeV, respectively.

Figures 1, 2, 3 and 4 show the number of MMs captured in the lifetime of the O+Ne (C+O) core high mass WDs samples [30] for model (I, II, III) as a function of t_9 due to RC effect when $m = 10^{15}$ GeV ($m = 10^{18}$ GeV), and $\sigma_m = 10^{-26}\,\mathrm{cm}^2$, $\phi_m = 10^{-26}\,\mathrm{cm}^{-2}\,\mathrm{s}^{-1}\,\mathrm{sr}^{-1}$ ($\phi_m = 10^{-28}\,\mathrm{cm}^{-2}\,\mathrm{s}^{-1}\,\mathrm{sr}^{-1}$) at the temperature of $T_6 = 0.1$, 1, 10, 100.

One find that as the t_9 increases, the number of MMs captured increases by about one order of magnitude. The longer the lifetime of the WDs, the more the number of the MMs captured becomes. For example, for model (II) in Fig. 1a, the number of MMs captured increases from 9.042×10^9 for O+Ne core mass WD J181913.36−120856.44 to 9.694×10^{10} for O+Ne core mass WD J055631.17+130639.78 when the t_9 increases from 0.37 to 3.33 at the temperature of $T_6 = 0.1$. However, at the same temperature for the same WDs, we have $N_2 > N_1 > N_3$. For instance, the number of MMs captured for WD J055631.17+130639.78 increases from $N_3 = 3.42 \times 10^6$ to $N_1 = 3.308 \times 10^{10}$, then further increases to $N_2 = 9.644 \times 10^{10}$.

As the temperature increases, the number of MMs captured has a little change. For example, when T_6 increases from 0.1 to 100, the number of MMs for model (II) increases about two orders of magnitude (i.e., N_2 increases from 9.694×10^{10} to 9.702×10^{12} for O+Ne core mass WD J055631.17+130639.78). However, for model (I, III), the temperature has no effect on the number of MMs captured due to the mass radius relation at zero temperature according to Eqs. (18, 20, 35, 37).

When we compare the results from Fig. 2 (4) with those of Fig. 1 (3), the number of MMs captured decreases 2 orders of magnitude due to $N \propto \phi_m$ (i.e., ϕ_m decreases from 10^{-26} to 10^{-28}).

When the temperature is certain, as the mass of the MM increases, the number of MMs captured increases. The higher the mass of the MM, the larger the number of MMs captured becomes from Figs. 1, 3 (2, 4). As the mass of MM increases from $m = 10^{15}$ GeV to $m = 10^{18}$ GeV, the number of MMs captured increases by 2, 3, and 4 orders of magnitude for model (I, II), and (III), respectively. For example, the number of the MMs captured increases from $N_1 = 3.308 \times 10^{10}$ to 2.577×10^{12}, $N_2 = 9.694 \times 10^{10}$ to 8.725×10^{13}, and $N_3 = 3.426 \times 10^6$ to 1.222×10^{10} for O+Ne core mass WD J055631.17+130639.78 for model (I), (II), and (II) at $T_6 = 0.1$, respectively. The reasons for this changes are not hard to understand according to Eqs. (3, 20, 24, 38). Based on same analysis for C+O core mass WD from Figs. 1, 2, 3

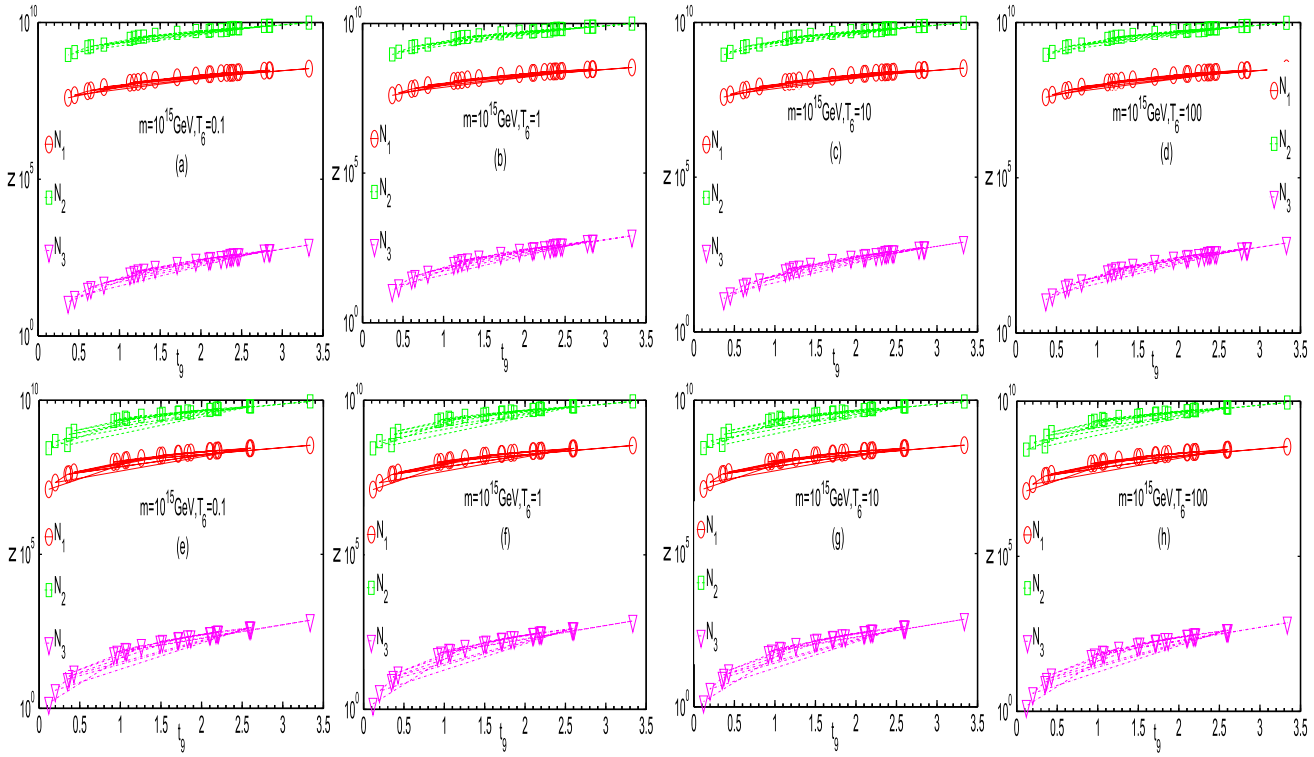

Fig. 2 The number of magnetic monopoles captured from space in the lifetime of the O+Ne (**a**–**d**) and C+O (**e**–**h**) core high mass WDs [30] for model (I, II, III) as a function of t_9 when $m = 10^{15}$ GeV, and $\sigma_m = 10^{-26}$ cm^2, $\phi_m = 10^{-28}$ cm^{-2} s^{-1} sr^{-1} at the temperature of $T_6 = 0.1, 1, 10, 100$

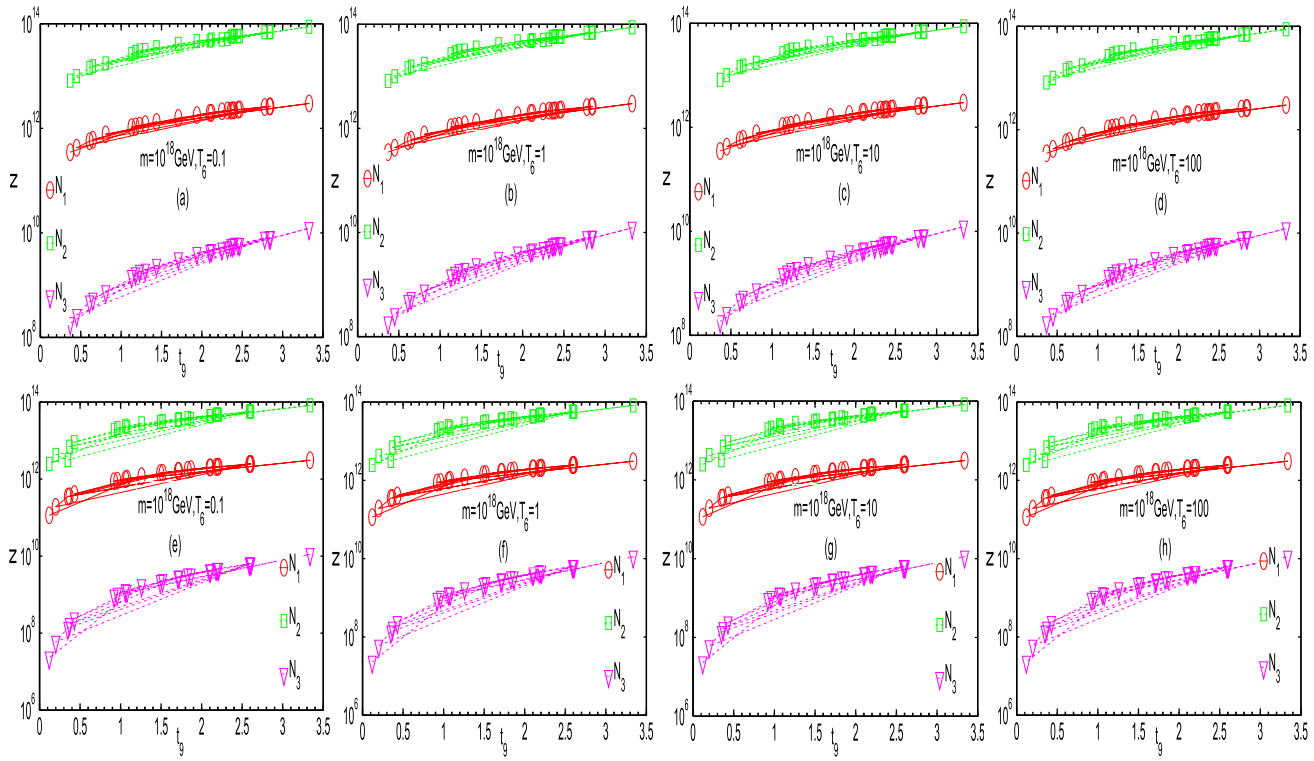

Fig. 3 The number of magnetic monopoles captured from space in the lifetime of the O+Ne (**a**–**d**) and C+O (**e**–**h**) core high mass WDs [30] for model (I, II, III) as a function of t_9 when $m = 10^{18}$ GeV, and $\sigma_m = 10^{-26}$ cm^2, $\phi_m = 10^{-26}$ cm^{-2} s^{-1} sr^{-1} at the temperature of $T_6 = 0.1, 1, 10, 100$

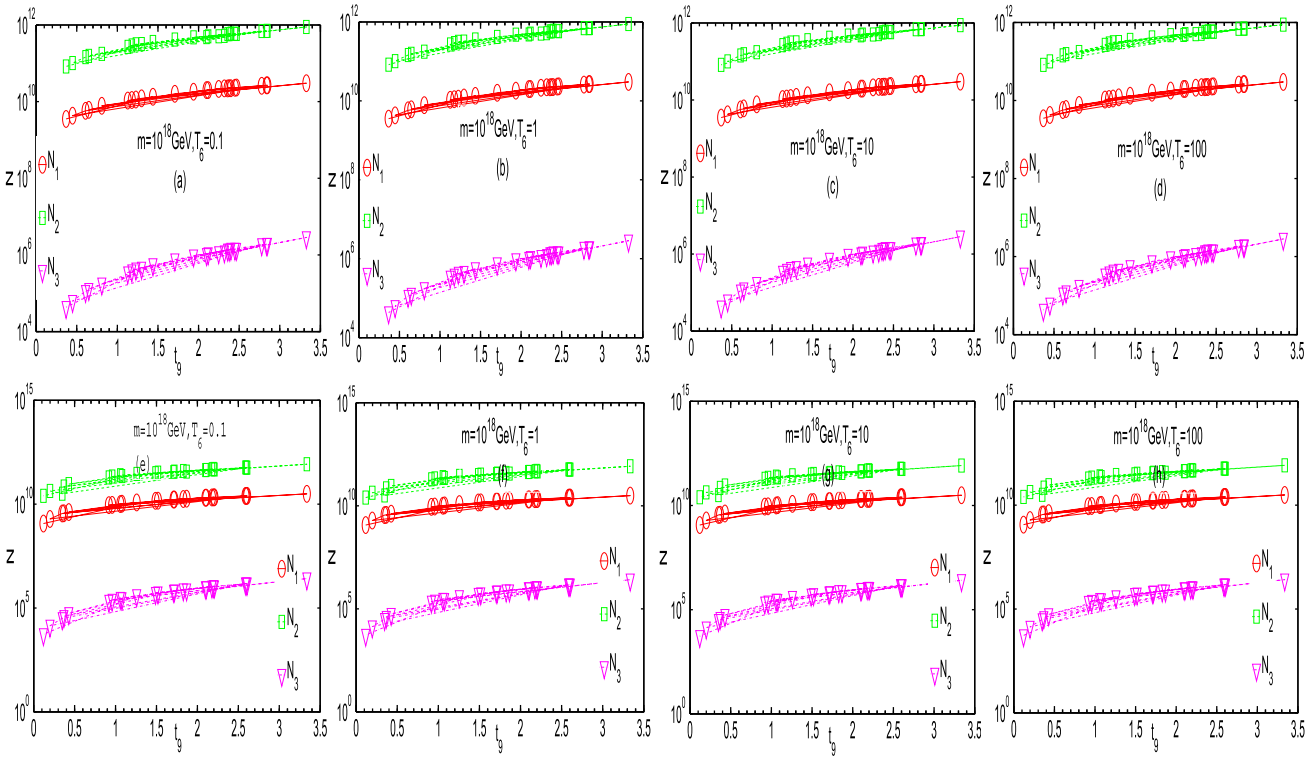

Fig. 4 The number of magnetic monopoles captured from space in the lifetime of the O+Ne (**a**–**d**) and C+O (**e**–**h**) core high mass WDs [30] for model (I, II, III) as a function of t_9 when $m = 10^{18}$ GeV, and $\sigma_m = 10^{-26}$ cm^2, $\phi_m = 10^{-28}$ cm^{-2} s^{-1} sr^{-1} at the temperature of $T_6 = 0.1, 1, 10, 100$

and 4 (e–h), we can obtain the results as same as those of O+Ne core mass WD.

Table 1 shows some information of the MMs capture by 25 typical high mass WDs selected from [30]. Tables 2 and 3 show the comparisons of model (II) of the number of MMs captured for O+Ne (C+O) core mass WD with those of model (I, III). One can find that $N_2 > N_1 > N_3$ on the same astronomical condition (e.g. CD_1). The maxnium of the number of MMs capture can be 9.6943×10^{11}, and 9.0671×10^{11} for O+Ne core high mass WD J055631.17+130639.78, and C+O core high mass WD J055631.17+130639.78, respectively.

Tables 4 and 5 show the comparisons of the number of MMs captured for WD-1136-286($M_* = 1.20$) of model (I, II, III) with those of [10] when $\sigma_m = 10^{-26}$, $t_9 = 6.47, 9.63$. N_2 is higher about by one order of magnitude than those of [10]. However, these are lower about 48%, and 1–2 orders of magnitude for N_1, and N_3, respectively. For example, in Table 4 (5), $k_3 = 0.010726(0.014227)$, and in Table 5, we can find that k_1 can get to 0.50614, 0.50449 for $m = 10^{17}$ GeV, $\beta = 10^{-3}$, and $m = 10^{18}$ GeV, $\beta = 10^{-3}$, respectively.

Possible causes of such above outcome can be from the effect of temperature on the WDs mass radius relation. The mass radius relation in model (I) is considered only on the condition of zero temperature according to classical formula Eq. (18). According to the Eq. (35), the mass radius relation in model (III) is considered on the condition of zero temperature, as well as the RC effect and the number of the MMs capture N_3 only for some lower mass WDs. It is found that, if a star contains a sufficient number of monopoles, its radius increases after some stage and finally it dissolves into a diffuse state. However, its lifetime is much longer than the age of the Universe because an energy source is rest mass, much larger than nuclear energy.

Traditional classical formula gives the problematic mass–radius relation $R \propto M^{1/3}$ (see Eq. (18)) for the low-density WDs because it leads to $R \to \infty$ and $p \to 0$ when $M \to 0$. Reference [46] corrected this mass–radius relation and obtained a reasonable formula (see Eq. (23)) in the relativistic WDs astronomical regions. Their results shown that the temperature effect mainly affected the middle- and low-density regions, and it could be above 10^7 K. Their results told us that the temperature effect on mass–radius relation was important for the low and middle central-density WDs. In model (II), the mass–radius relation of the WDs derived according to statistical mechanics. The temperature effect has to be considered.

On the other hand, according to stellar evolution theory, radiative transfer of energy is negligible compared with thermal conduction in the highly degenerate core of WDs, in spite of the reduced opacity of a degenerate gas. It will be shown that the thermal conduction is so great that, during the cooling

Table 1 Some information of O+Ne core and C+O core high mass white dwarf samples from [30]

Star	Star name	Compsition	O+Ne core			C+O core		
			M_*	$T_{\rm eff}$	T_9	M_*	$T_{\rm eff}$	T_9
1	WD J010338.56−052251.96	H	1.262	9040	2.84	1.310	9110	2.60
2	WD J025431.45+301935.38	logH/He = − 5	1.302	11060	2.25	1.330	11620	1.49
3	SDSS J114012.81+232204.7	H	1.294	11860	2.10	1.336	12080	1.71
4	SDSS J132926.04+254936.4	H	1.314	29010	0.81	1.351	29760	0.37
5	SDSS J172736.28+383116.9	H	1.252	9420	2.78	1.302	9420	2.59
6	WD J183202.83+085636.24	He	1.310	34210	0.45	1.319	34410	0.20
7	WD J190132.74+145807.18	H	1.279	29100	0.61	1.422	30200	0.35
8	SDSS J221141.80+113604.5	H	1.262	9020	2.85	1.314	9180	2.61
9	SDSS J225513.48+071000.9	H	1.264	10990	2.36	1.313	11150	2.18
10	SDSS J235232.30−025309.2	H	1.272	10680	2.38	1.329	10780	2.10
11	WD J004917.14−252556.81	H	1.263	13020	1.94	1.322	13480	1.72
12	WD J032900.79−212309.24	H	1.315	10330	2.32	1.344	10620	1.87
13	WD J042642.02−502555.21	H	1.266	17900	1.30	1.328	19470	1.08
14	WD J043952.72+454302.81	H	1.258	19120	1.18	1.307	19750	0.96
15	WD J055631.17+130639.78	H	1.207	8340	3.33	1.257	10940	3.34
16	WD J060853.60−451533.03	H	1.279	19580	1.13	1.326	21490	0.92
17	WD J070753.00+561200.25	H	1.240	18100	1.23	1.291	18450	1.06
18	WD J080502.93−170216.57	H	1.254	10830	2.40	1.304	10830	2.20
19	WD J093430.71−762614.48	H	1.284	10050	2.47	1.328	10160	2.11
20	WD J095933.33−182824.16	H	1.278	12000	2.12	1.320	13350	1.83
21	WD J111646.44−160329.42	H	1.271	10480	2.45	1.325	10660	2.21
22	WD J125428.86−045227.48	H	1.266	14420	1.71	1.318	14590	1.52
23	WD J174441.56−203549.05	H	1.275	27140	0.65	1.320	28030	0.43
24	SDSS J180001.21+451724.7	H	1.253	16410	1.44	1.303	16600	1.26
25	WD J181913.36−120856.44	H	1.305	37970	0.37	1.327	39910	0.12

of a WD, the temperature is always very nearly uniform in the core. Monopoles trapped inside WDs can catalyze decay of nucleons and provide an additional source of internal heat for the star. A monopole which passes through WDS can easily lose enough energy to be captured. Ahlen and Kinoshita [40] calculated these energy source, which comes from the electronic interactions and given by $dE/dx \approx 100\rho\beta$ GeV/cm, where ρ is the density of the WD (in g cm^{-3}), and $\beta = v_m/c$ is the ratio of the velocity of the MM to light velocity as it passes through the WDs [**?**]. Far from the WD the velocity of the typical monopole in the galaxy is the virial velocity (i.e., $v_m = 10^{-3}c$). When a MM falls into the gravitational potential well of the WDs, it is accelerated and β increase to $(v_m^2 + 2GM/R)^{1/2}$ at the surface of WDs. The energy loss in traveling through the WDs can be about 5×10^{17} MeV. Once the monopole is captured, it sinks toward the center of the WDs. If we consider the motion of a monopole as a harmonic oscillator with a dE/dX damping term, then the time scale for the monopole to fall from rest to the center can be estimated to be about 1000s.

5.2 The comparision of the luminosities with the WD observations

Figures 5, 6, 7 and 8 show the luminosities of the O+Ne (C+O) core high mass WDs samples [30] for model (I, II, III) as a function of t_9 due to RC effect when $m = 10^{15}$ GeV ($m = 10^{18}$ GeV), and $\sigma_m = 10^{-26}\,\mathrm{cm}^2$, $\phi_m = 10^{-26}\,\mathrm{cm}^{-2}\,\mathrm{s}^{-1}\,\mathrm{sr}^{-1}$ ($\phi_m = 10^{-28}\,\mathrm{cm}^{-2}\,\mathrm{s}^{-1}\,\mathrm{sr}^{-1}$) at the temperature of $T_6 = 0.1, 1, 10, 100$.

We find that the luminosities for WDs increase about by one order magnitude as the t_9 increases for model (I) and (II), but decrease about by one order magnitude for model (III). For example, from Fig. 5a the luminosities increase from 1.825×10^{29} to 1.334×10^{30}, and from 1.825×10^{29} to 1.334×10^{30}, for model (I), and (II), respectively when t_9 increases from 0.37(for WD J181913.36 − 120856.44) to 3.33 (for WD J055631.17+130639.78), but decrease from 2.343×10^{30} to 2.887×10^{29} for model (III).

On the other hand, when the temperature increases from $T_9 = 0.01$ to $T_6 = 100$, for the same WDs, the luminosities increase about by 1–2 orders of magnitude. For example,

Table 2 The number of MMs captured in the space of O+Ne core high mass WDs when $T_6 = 10$, and $\sigma_m = 10^{26}\text{cm}^2$. Some typical astronomical conditions of CD_i (i=1, 2, 3, 4) are noted as $m = 10^{15}$ GeV, $\phi_m = 10^{-26}\,\text{cm}^{-2}\,\text{s}^{-1}\,\text{sr}^{-1}$; $m = 10^{15}$ GeV, $\phi_m = 10^{-28}\,\text{cm}^{-2}\,\text{s}^{-1}\,\text{sr}^{-1}$; $m = 10^{18}$ GeV, $\phi_m = 10^{-26}\,\text{cm}^{-2}\,\text{s}^{-1}\,\text{sr}^{-1}$; $m = 10^{18}$ GeV, $\phi_m = 10^{-26}\,\text{cm}^{-2}\,\text{s}^{-1}\,\text{sr}^{-1}$, respectively

Star	CD_1			CD_2			CD_3			CD_4		
	N_1	N_2	N_3	N_1	N_2	N_3	N_1	N_2	N_3	N_1	N_2	N_3
1	2.9062e10	7.6416e11	2.2954e6	2.9062e8	7.6416e9	5.3027e3	2.6156e12	6.8774e13	8.2041e9	2.6156e10	6.8774e11	1.8953e6
2	2.3508e10	5.5431e11	1.3922e6	2.3508e8	5.5431e9	3.2163e3	2.1158e12	4.9888e13	4.9760e9	2.1158e10	4.9888e11	1.1495e6
3	2.1851e10	5.2805e11	1.2468e6	2.1851e8	5.2805e9	2.8803e3	1.9666e12	4.7524e13	4.4563e9	1.9666e10	4.7524e11	1.0295e6
4	8.5150e9	1.9288e11	2.1243e5	8.5150e7	1.9288e9	4.9074e3	7.6635e11	1.7359e13	7.5925e8	7.6635e9	1.7359e11	1.7540e5
5	2.8298e10	7.6111e11	2.2516e6	2.8298e8	7.6111e9	5.2014e3	2.5468e12	6.8500e13	8.0473e9	2.5468e10	6.8500e11	1.8590e6
6	4.6993e9	1.1116e11	7.4762e4	4.6993e7	1.1116e9	1.7271e3	4.2294e11	1.0004e13	2.6721e8	4.2294e9	1.0004e11	6.1728e4
7	6.2981e9	1.5874e11	1.3554e5	6.2981e7	1.5874e9	3.1312e3	5.6683e11	1.4286e13	4.8444e8	5.6683e9	1.4286e11	1.1191e5
8	2.9164e10	7.6685e11	2.3101e6	2.9164e8	7.6685e9	5.3367e3	2.6248e12	6.9016e13	8.2567e9	2.6248e10	6.9016e11	1.9074e6
9	2.4176e10	6.3268e11	1.6330e6	2.4176e8	6.3268e9	3.7724e3	2.1758e12	5.6941e13	5.8365e9	2.1758e10	5.6941e11	1.3483e6
10	2.4483e10	6.2832e11	1.6327e6	2.4483e8	6.2832e9	3.7719e3	2.2035e12	5.6549e13	5.8356e9	2.2035e10	5.6549e11	1.3481e6
11	1.9863e10	5.2104e11	1.1457e6	1.9863e8	5.2104e9	2.6468e3	1.7876e12	4.6894e13	4.0949e9	1.7876e10	4.6894e11	9.4598e5
12	2.4277e10	5.6694e11	1.4637e6	2.4277e8	5.6694e9	3.3814e3	2.1849e12	5.1025e13	5.2315e9	2.1849e10	5.1025e11	1.2085e6
13	1.3331e10	3.4721e11	5.5010e5	1.3331e8	3.4721e9	1.2708e3	1.1998e12	3.1249e13	1.9661e9	1.1998e10	3.1249e11	4.5420e5
14	1.2050e10	3.1978e11	4.6852e5	1.2050e8	3.1978e9	1.0823e3	1.0845e12	2.8780e13	1.6745e9	1.0845e10	2.8780e11	3.8684e5
15	3.3079e10	9.6943e11	3.4202e6	3.3079e8	9.6943e9	7.9010e3	2.9771e12	8.7249e13	1.2224e10	2.9771e10	8.7249e11	2.8239e6
16	1.1667e10	2.9405e11	4.1581e5	1.1667e8	2.9405e9	9.6056e3	1.0500e12	2.6465e13	1.4861e9	1.0500e10	2.6465e11	3.4332e5
17	1.2440e10	3.4316e11	5.2343e5	1.2440e8	3.4316e9	1.2092e3	1.1196e12	3.0885e13	1.8708e9	1.1196e10	3.0885e11	4.3218e5
18	2.4456e10	6.5488e11	1.7168e6	2.4456e8	6.5488e9	3.9660e3	2.2010e12	5.8939e13	6.1360e9	2.2010e10	5.8939e11	1.4175e6
19	2.5569e10	6.3580e11	1.7069e6	2.5569e8	6.3580e9	3.9433e3	2.3012e12	5.7222e13	6.1008e9	2.3012e10	5.7222e11	1.4094e6
20	2.1877e10	5.5284e11	1.3078e6	2.1877e8	5.5284e9	3.0213e3	1.9689e12	4.9756e13	4.6744e9	1.9689e10	4.9756e11	1.0798e6
21	2.5190e10	6.4808e11	1.7244e6	2.5190e8	6.4808e9	3.9837e3	2.2671e12	5.8328e13	6.1633e9	2.2671e10	5.8328e11	1.4238e6
22	1.7536e10	4.5672e11	9.0553e5	1.7536e8	4.5672e9	2.0919e3	1.5782e12	4.1105e13	3.2365e9	1.5782e10	4.1105e11	7.4767e5
23	6.6971e9	1.7056e11	1.5331e5	6.6971e7	1.7056e9	3.5416e3	6.0274e11	1.5351e13	5.4794e8	6.0274e9	1.5351e11	1.2658e5
24	1.4666e10	3.9359e11	6.7953e5	1.4666e8	3.9359e9	1.5698e3	1.3199e12	3.5423e13	2.4287e9	1.3199e10	3.5423e11	5.6107e5
25	3.8718e9	9.0417e11	5.1981e4	3.8718e7	9.041708	1.2008e3	3.4846e11	8.1375e12	1.8579e8	3.4846e9	8.1375e10	4.2919e4

Table 3 The number of MMs captured in the space of C+O core high mass WDs when $T_6 = 10$, and $\sigma_m = 10^{-26}\text{cm}^2$. Some typical astronomical conditions of CD_i (i=1, 2, 3, 4) are noted as $m = 10^{15}$ GeV, $\phi_m = 10^{-26}\,\text{cm}^{-2}\,\text{s}^{-1}\,\text{sr}^{-1}$; $m = 10^{15}$ GeV, $\phi_m = 10^{-28}\,\text{cm}^{-2}\,\text{s}^{-1}\,\text{sr}^{-1}$; $m = 10^{18}$ GeV, $\phi_m = 10^{-26}\,\text{cm}^{-2}\,\text{s}^{-1}\,\text{sr}^{-1}$; $m = 10^{18}$ GeV, $\phi_m = 10^{-26}\,\text{cm}^{-2}\,\text{s}^{-1}\,\text{sr}^{-1}$, respectively

Star	CD_1			CD_2			CD_3			CD_4		
	N_1	N_2	N_3	N_1	N_2	N_3	N_1	N_2	N_3	N_1	N_2	N_3
1	2.7276e10	6.2648e11	1.7838e6	2.7276e8	6.2648e9	4.1209e3	2.4549e12	5.6383e13	6.3756e9	2.4549e10	5.6383e11	1.4728e6
2	1.5790e10	3.3658e11	6.2458e5	1.5790e8	3.3658e9	1.4429e3	1.4211e12	3.0292e13	2.2323e9	1.4211e10	3.0292e11	5.1569e5
3	1.8176e10	3.7771e11	7.9348e5	1.8176e8	3.7771e9	1.8330e3	1.6359e12	3.3994e13	2.8360e9	1.6359e10	3.3994e11	6.5515e5
4	3.9622e9	7.6668e10	4.7744e4	3.9622e7	7.6668e8	1.1029e3	3.5660e11	6.9001e12	1.7064e8	3.5660e9	6.9001e19	3.9420e4
5	2.7061e10	6.3807e11	1.7982e6	2.7061e8	6.3807e9	4.1541e3	2.4355e12	5.7427e13	6.4270e9	2.4355e10	5.7427e11	1.4847e6
6	2.1078e9	4.6893e10	1.6546e4	2.1078e7	4.6893e8	3.8224e3	1.8970e11	4.2204e12	5.9138e7	1.8970e9	4.2204e10	1.3662e4
7	3.8782e9	3.4773e10	3.8057e4	3.8782e7	3.4773e8	8.7917e3	3.4904e11	3.1296e12	1.3602e8	3.4904e9	3.1296e10	3.1423e4
8	2.7437e10	6.2151e11	1.7829e6	2.7437e8	6.2151e9	4.1188e3	2.4693e12	5.5936e13	6.3724e9	2.4693e10	5.5936e119	1.4721e6
9	2.2905e10	5.2067e11	1.2876e6	2.2905e8	5.2067e9	2.9746e3	2.0615e12	4.6860e13	4.6021e9	2.0615e10	4.6860e11	1.0632e6
10	2.2244e10	4.7607e11	1.1678e6	2.2244e8	4.7607e9	2.6977e3	2.0019e12	4.2846e13	4.1737e9	2.0019e10	4.2846e11	9.6419e5
11	1.8154e10	3.9938e11	8.2294e5	1.8154e8	3.9938e9	1.9011e3	1.6339e12	3.5944e13	2.9413e9	1.6339e10	3.5944e11	6.7947e5
12	1.9956e10	3.9983e11	9.2002e5	1.9956e8	3.9983e9	2.1254e3	1.7960e12	3.5984e13	3.2883e9	1.7960e10	3.5984e11	7.5963e5
13	1.1434e10	2.4571e11	3.4920e5	1.1434e8	2.4571e9	8.0607e3	1.0290e12	2.2114e13	1.2481e9	1.0290e10	2.2114e11	2.8832e5
14	1.0056e10	2.333e11	2.9313e5	1.0056e8	2.333e9	6.7718e3	9.0503e11	2.0997e13	1.0477e9	9.0503e9	2.0997e11	2.4203e5
15	3.4088e10	9.0671e11	3.1128e6	3.4088e8	9.0671e9	7.1909e3	3.0679e12	8.1603e13	1.1125e10	3.0679e10	8.1603e11	2.5701e6
16	9.7301e9	2.1077e11	2.6186e5	9.7301e7	2.1077e9	6.0494e3	8.7571e11	1.8969e13	9.3593e8	8.7571e9	1.8969e11	2.1621e5
17	1.1013e10	2.6848e11	3.6178e5	1.1013e8	2.6848e9	8.3575e3	9.9114e11	2.4163e13	1.2930e9	9.9114e9	2.4163e11	2.9871e5
18	2.3010e10	5.3909e11	1.3315e6	2.3010e8	5.3909e9	3.0759e3	2.0709e12	4.8518e13	4.7589e9	2.0709e10	4.8518e11	1.0994e6
19	2.2338e10	4.8004e11	1.1801e6	2.2338e8	4.8004e9	2.7261e3	2.0104e12	4.3203e13	4.2177e9	2.0104e10	4.3203e11	9.7435e5
20	1.9296e10	4.277e11	9.2455e5	1.9296e8	4.2773e9	2.1358e3	1.7366e12	3.8493e13	3.3045e9	1.7366e10	3.8493e11	7.6337e5
21	2.3362e10	5.0804e11	1.2909e6	2.3362e8	5.0804e9	2.9821e3	2.1025e12	4.5723e13	4.6137e9	2.1025e10	4.5723e11	1.0658e6
22	1.6011e10	3.5752e11	6.6220e5	1.6011e8	3.5752e9	1.5298e3	1.4410e12	3.2176e13	2.3668e9	1.4410e10	3.2176e11	5.4676e5
23	4.5340e9	1.0050e11	6.6424e4	4.5340e7	1.0050e9	1.5345e3	4.0806e11	9.0448e12	2.3741e8	4.0806e9	9.0448e10	5.4844e6
24	1.3171e10	3.0958e11	4.8424e05	1.3171e8	3.0958e9	1.1187e3	1.1854e12	2.7863e13	1.7307e9	1.1854e10	2.7863e11	3.9982e6
25	1.2698e9	2.7396e10	6.4401e3	1.2698e7	2.7396e8	1.4878e3	1.1428e11	2.4657e12	2.3018e7	1.1428e9	2.4657e11	5.3174e5

Table 4 The comparisons of the number of MMs captured and the upper limits of the MMs flux ϕ_m with those of [10] (N_m(FK), and ϕ_m(FK)) of WD-1136-286($M_* = 1.20$, $t_9 = 6.47$, $T_{eff} = 4490$) when $\sigma_m = 10^{-26}\text{cm}^2$ and $k_i (i = 1, 2, 3) = N_i/N_m(\text{FK})$, $k_j (j = 4, 5, 6) = \phi_{m(1,2,3)}/\phi_m(\text{FK})$. Our upper limits of the MMs flux ϕ_{m1}, ϕ_{m2}, and ϕ_{m3} are corresponding to the results for model (I,II,III)

m (GeV)	β	N_m(FK)	N_1	N_2	N_3	ϕ_m(FK)	ϕ_{m1}	ϕ_{m2}	ϕ_{m3}	k_1	k_2	k_3	k_4	k_5	k_6
1.0e15	1.0e−2	3.100e7	1.6133e7	4.7823e8	3.3252e5	2.80e−30	3.2473e−30	1.9728e−24	4.6880e−23	0.5204	15.427	0.0107	1.1598	7.0457e5	1.6743e7
1.0e16	3.0e−3	3.470e8	1.8502e8	5.4896e9	2.8065e7	2.89e−30	1.0269e−31	6.2500e−26	2.8622e−23	0.5332	15.82	0.0809	3.5500e−2	2.1626e4	9.9038e6
1.0e17	1.0e−3	1.283e9	6.7415e8	2.0002e10	2.9453e8	1.17e−30	3.6081e−31	2.1920e−26	5.2088e−25	0.5255	15.59	0.2296	3.0800e−1	1.8735e4	4.4520e5
1.0e18	1.0e−3	3.667e9	1.9187e9	5.6928e10	1.9727e9	3.33e−30	1.1410e−30	6.9445e−27	3.1802e−24	0.5232	15.524	0.5380	3.4000e−1	2.0854e3	9.5502e5

Table 5 The comparisons of the number of MMs captured and the upper limits of the MMs flux ϕ_m with those of [10] (N_m(FK), and ϕ_m(FK)) of WD-1136-286($M_* = 1.20$, $t_9 = 9.63$, $T_{eff} = 4490$) when $\sigma_m = 10^{-26}\text{cm}^2$ and $k_i (i = 1, 2, 3) = N_i/N_m(\text{FK})$, $k_j (j = 4, 5, 6) = \phi_{m(1,2,3)}/\phi_m(\text{FK})$. Our upper limits of the MMs flux ϕ_{m1}, ϕ_{m2}, and ϕ_{m3} are corresponding to the results for model (I,II,III)

m (GeV)	β	N_m(FK)	N_1	N_2	N_3	ϕ_m(FK)	ϕ_{m1}	ϕ_{m2}	ϕ_{m3}	k_1	k_2	k_3	k_4	k_5	k_6
1.0e15	1.0e−2	4.600e7	2.3413e7	6.9465e8	6.5443e5	2.73e−30	2.1817e−30	1.3254e−24	3.1496e−23	0.5090	15.101	0.0142	7.9916e−1	4.8549e5	1.1537e7
1.0e16	3.0e−3	4.800e8	2.5442e8	7.5487e9	5.0083e7	2.67e−30	6.8992e−31	4.1991e−26	1.9230e−23	0.5300	15.726	0.1043	2.5840e−1	1.5727e4	7.2022e6
1.0e17	1.0e−3	1.813e9	9.1764e8	2.7226e10	5.1597e8	1.07e−30	2.4241e−31	1.4727e−26	3.4996e−25	0.5061	15.017	0.2846	2.2655e−1	1.3764e4	3.2707e5
1.0e18	1.0e−3	4.590e10	2.3156e10	6.8702e11	1.8268e10	2.70e−29	7.6658e−31	4.6657e−27	2.1367e−24	0.5045	14.968	0.3980	2.8392e−2	1.7280e2	7.9137e4

the luminosities from Fig. 5 for WD J181913.36−120856.44 increase from 1.825×10^{29} to 5.770×10^{30}, 7.743×10^{28} to 2.444×10^{30}, and 2.343×10^{30} to 6.939×10^{31} for model (I, II, III), respectively. To compare the luminosities of model (I) with those of model (II), the luminosities of model (I) are agreed well with those of model (II) from Figs. 5, 6, 7 and 8. The difference between the two models is no more than one order of magnitude. The luminosities for model (III) can be higher about by 1–2 orders of magnitude than those of model (I, II) for some relativistic lower lifetime WDs (e.g., $t_9 = 0.37$). However, as the lifetime increases, for some higher lifetime WDs the difference will change smaller and smaller. From the comparisons of the luminosities of observation $L_{\rm rad}$ with those of model (I, II, III), we find that the difference is no more than three orders magnitude. For example, the difference between the observation $L_{\rm rad}$ and the luminosities for the three model are about 2, 3, 1 orders magnitude at $T_6 = 0.01$ for high mass O+Ne core WD J181913.36−120856.44 from Fig. 5a.

The luminosities of O+Ne (C+O) core high mass WDs are given in Tables 6, 7 (or 8, 9) when $T_6 = 0.1, 100$, and $\sigma_m = 10^{-26}{\rm cm}^2$. From Tables 6, 7, 8 and 9, when other parameters are certain, with the decreasing of the flux of MMs (e.g., ϕ_m from 10^{-26} to 10^{-28}), the luminosities for model (I, II) decrease due to $L_m \propto \phi_m$ according to Eqs. (22, 26), but increase for model (III) according to Eq. (39) (e.g., for the condition $CD_1 \rightarrow CD_2$). The results from these Figures, on the other hand, show that the luminosities increase as the mass of MM increases (e.g, from 10^{15} GeV to 10^{18} GeV) for model (I, II), but decrease for model (III). This is because that the mass radius relation is strongly effected by the number MMs captured in model (III) according Eq. (35).

Tables 6, 7, 8 and 9 also show the comparisons of the observations with the luminosities for the three models. We find that the luminosities of the observations ($L_{\rm rad}$) are the range from 1.70134×10^{29} (i.e., for WD J055631.17+130639.78) to 4.9391×10^{31} (i.e., for WD J181913.36−120856.44), and 2.2935×10^{29} (i.e., for WD J010338.56−052251.96) to 8.3758×10^{31} (i.e., for WD J181913.36−120856.44) for O+Ne, and C+O core high mass WDs, respectively. From Tables 6 and 7, the ranges of the luminosities are $3.1063 \times 10^{27} \leq L_1 \leq 2.0788 \times 10^{33}$, $1.3410 \times 10^{27} \leq L_2 \leq 7.5678 \times 10^{32}$, and $2.8533 \times 10^{29} \leq L_3 \leq 7.6029 \times 10^{32}$ for O+Ne WDs for model (I, II, III), respectively. Based on the calculations from Tables 8 and 9, the ranges of the luminosities are $1.0717 \times 10^{27} \leq L_1 \leq 2.3234 \times 10^{33}$, $5.3278 \times 10^{26} \leq L_2 \leq 9.7377 \times 10^{32}$, and $4.0886 \times 10^{29} \leq L_3 \leq 1.08066 \times 10^{32}$ for C+O core WDs for model (I, II, III), respectively.

From the above analysis, it is shown that the luminosities for model (III) are agreed well with the observations and the differences are about one order of magnitude. However, the observations $L_{\rm rad}$ can be 2 and 2–3 orders magnitude lower than those of model (I), and (II), respectively.

5.3 The comparision of the limit of the flux of MMs with previous calculations

The mass and the flux of MMs are always the open and interesting questions for physicist and astrophysicist. Grand unification theories (GUTs) suggested that massive MMs (mass $\sim 10^{16}$ GeV) were created in the very early stages of the formation of the Universe. The problem of the flux of the MM has attracted many physicists and astrophysicists to work on it.

By requiring survival of μG magnetic fields observed in our Galaxy, [36] obtained the limit of the flux of MMs and gave $\phi_m \leq 10^{-16}\,{\rm cm}^{-2}\,{\rm sr}^{-1}\,{\rm s}^{-1}$. Due to acceleration by the galactic magnetic field, subsequently, [35] gave an improvement on this work by considering the effect of the monopole mass and velocity. They shown the limit of the flux of the MMs was $\phi_m \leq 10^{-12}\,{\rm cm}^{-2}\,{\rm sr}^{-1}\,{\rm s}^{-1}$ for the MM's mass of $\sim 10^{19}$ GeV with the velocity of $\sim 10^{-3}c$. [48] discussed the problem on the flux of the MMs. They presented a new limit on the MM's flux, which is less than $4.1 \times 10^{-13}\,{\rm cm}^{-2}\,{\rm sr}^{-1}\,{\rm s}^{-1}$ for the velocity in the range from 0.001 c to 0.01 c. Then [49] described the results of six months observations with a large inductive detector and proposed a new upper bound on the flux of cosmic MMs. The experimental upper bound on the flux could be $6 \times 10^{-12}\,{\rm cm}^{-2}\,{\rm sr}^{-1}\,{\rm s}^{-1}$. Adams et al. [50] extended Parker bound and gave another improvement on this work. Their discussions shown that the flux of the MMs was $\phi_m \leq 1.2 \times 10^{-16}(m/10^{17}\,{\rm GeV}){\rm cm}^{-2}\,{\rm sr}^{-1}\,{\rm s}^{-1}$. However, on the basis of the above analysis, they all lost sight of the RC effect on the flux.

MMs flux limits from catalysis of nucleon decay was discussed by [51]. Their results shown that the upper flux of the MMs was $\phi_m \leq 8.7 \times 10^{-14}\,{\rm cm}^{-2}\,{\rm sr}^{-1}\,{\rm s}^{-1}$, and $\phi_m \leq 2.2 \times 10^{-15}\,{\rm cm}^{-2}\,{\rm sr}^{-1}\,{\rm s}^{-1}$ when $5 \times 10^{-3} \leq \beta \leq 5 \times 10^{-2}$ at the monopole catalysis interaction mean free path $\lambda_c = 100$, 10m, respectively. On the other hand, the upper flux of the MMs could be $\phi_m \leq 8.7 \times 10^{-16}\,{\rm cm}^{-2}\,{\rm sr}^{-1}\,{\rm s}^{-1}$, and $\phi_m \leq 8.0 \times 10^{-16}\,{\rm cm}^{-2}\,{\rm sr}^{-1}\,{\rm s}^{-1}$ when $10^{-3} \leq \beta \leq 10^{-1}$, and $10^{-4} \leq \beta \leq 10^{-1}$ at $\lambda_c = 1.0$, 0.1m, respectively.

Becker-Szendy et al. [52] also discussed the MM's flux limits from the IMB proton decay detector. They obtained that the upper flux of the MMs could be $\phi_m \leq 2.7 \times 10^{-15}\,{\rm cm}^{-2}\,{\rm sr}^{-1}\,{\rm s}^{-1}$, and $\phi_m \leq 1.0 \times 10^{-15}\,{\rm cm}^{-2}\,{\rm sr}^{-1}\,{\rm s}^{-1}$ when $\beta \leq 10^{-3}$, for $\sigma_m = 10^{-24}{\rm cm}^2$, and $\sigma_m = 10^{-25}{\rm cm}^2$, respectively.

Catalysis of nucleon decay in WDs is used to constrain the abundance of MMs arising from grand unified theories. The flux of MMs from catalysis of nucleon decay in WDs was discussed by [10]. Their results shown

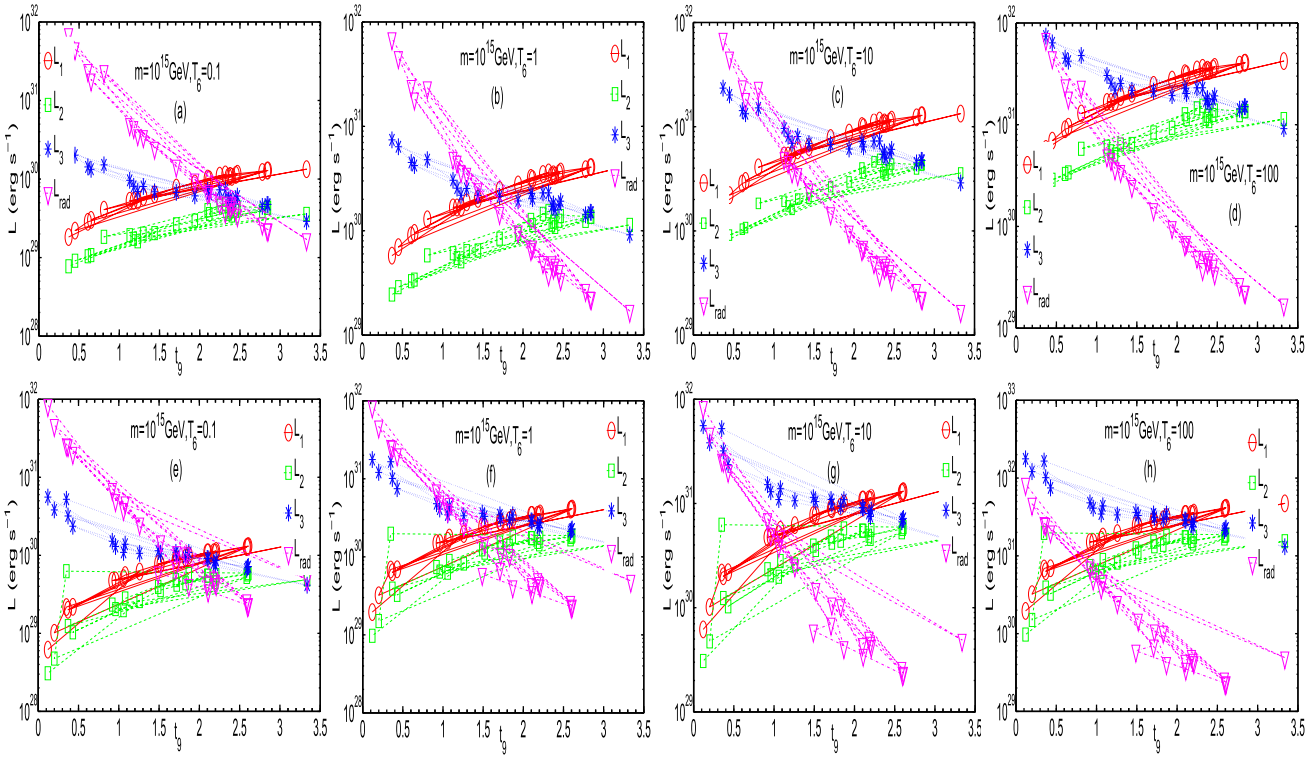

Fig. 5 The luminosities as a function of T_9 for the O+Ne (**a**–**d**) and C+O (**e**–**h**) core high mass WDs [30] when $m = 10^{15}$ GeV, and $\sigma_m = 10^{-26}$ cm^2, $\phi_m = 10^{-26}$ cm^{-2} s^{-1} sr^{-1} at the temperature of $T_6 = 0.1, 1, 10, 100$

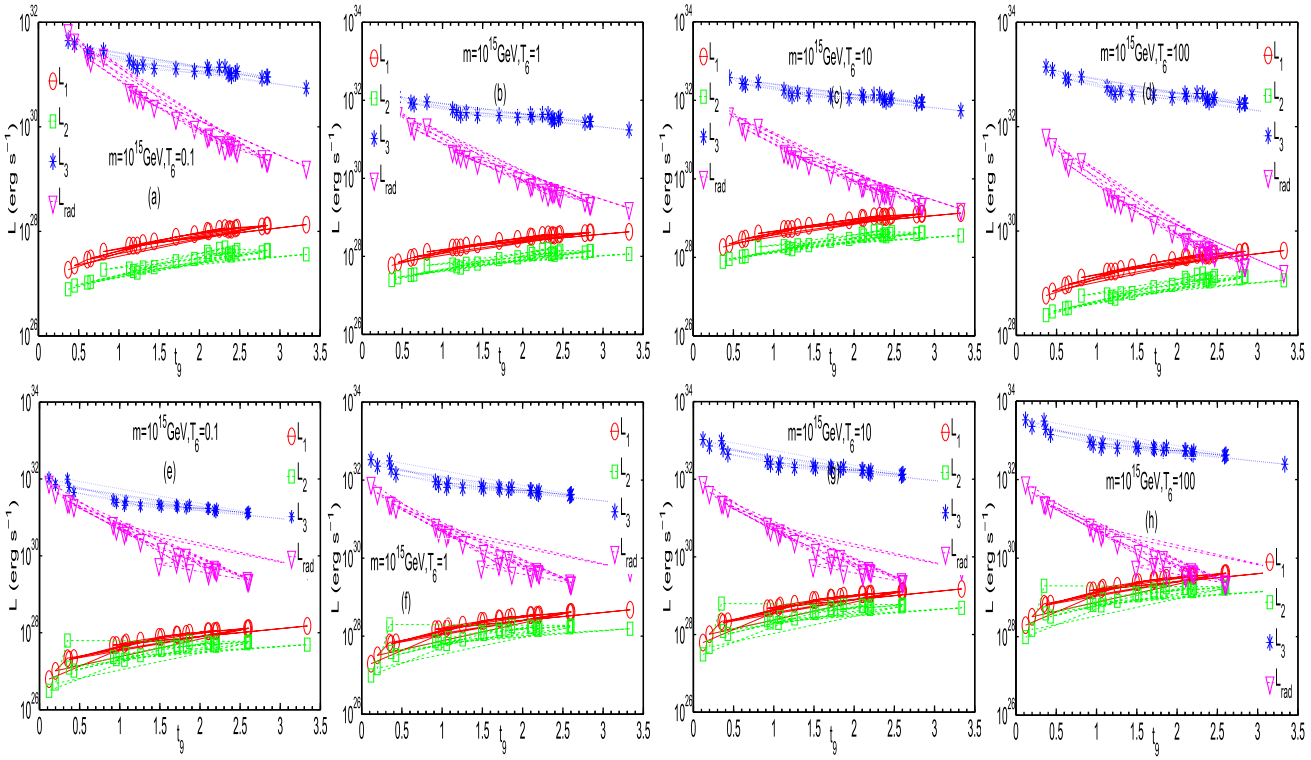

Fig. 6 The luminosities as a function of T_9 for the O+Ne (**a**–**d**) and C+O (**e**–**h**) core high mass WDs [30] when $m = 10^{15}$ GeV, and $\sigma_m = 10^{-26}$ cm^2, $\phi_m = 10^{-28}$ cm^{-2} s^{-1} sr^{-1} at the temperature of $T_6 = 0.1, 1, 10, 100$

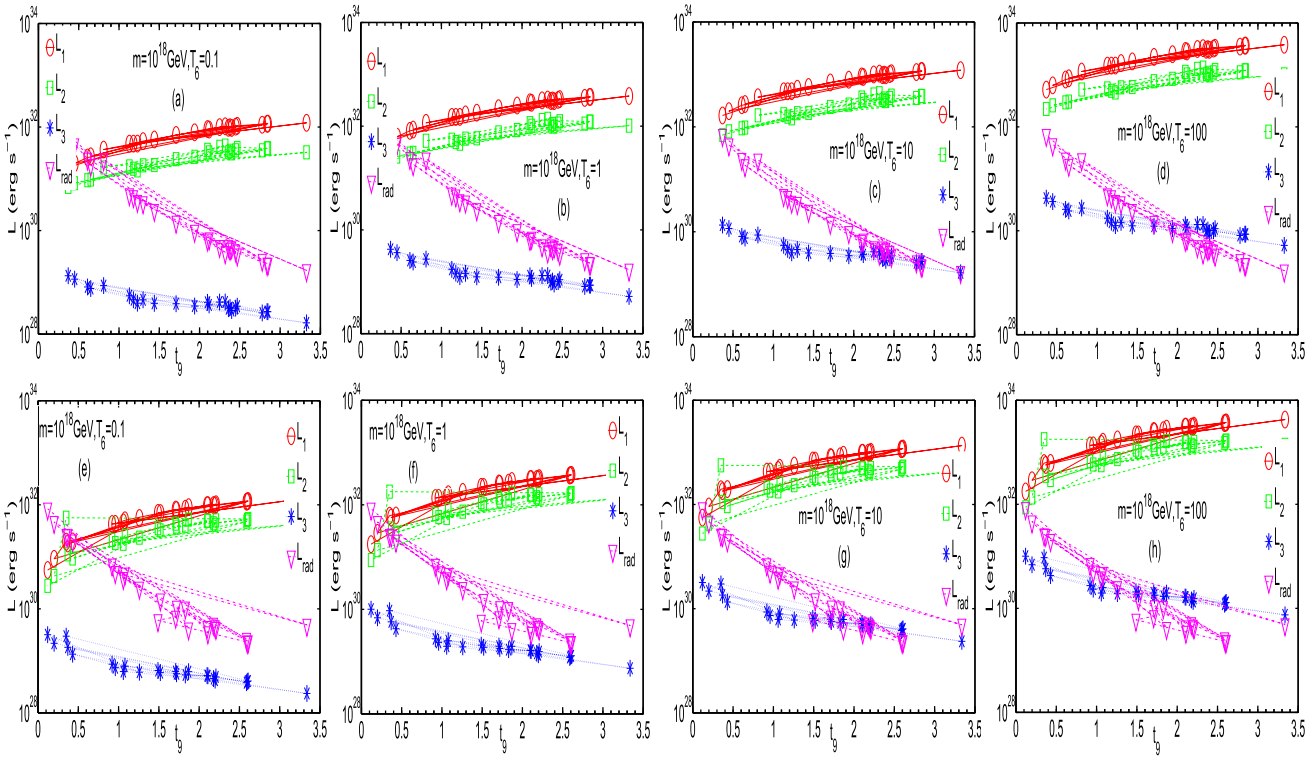

Fig. 7 The luminosities as a function of T_9 for the O+Ne (**a**–**d**) and C+O (**e**–**h**) core high mass WDs [30] when $m = 10^{18}$ GeV, and $\sigma_m = 10^{-26}$ cm^2, $\phi_m = 10^{-26}$ cm^{-2} s^{-1} sr^{-1} at the temperature of $T_6 = 0.1, 1, 10, 100$

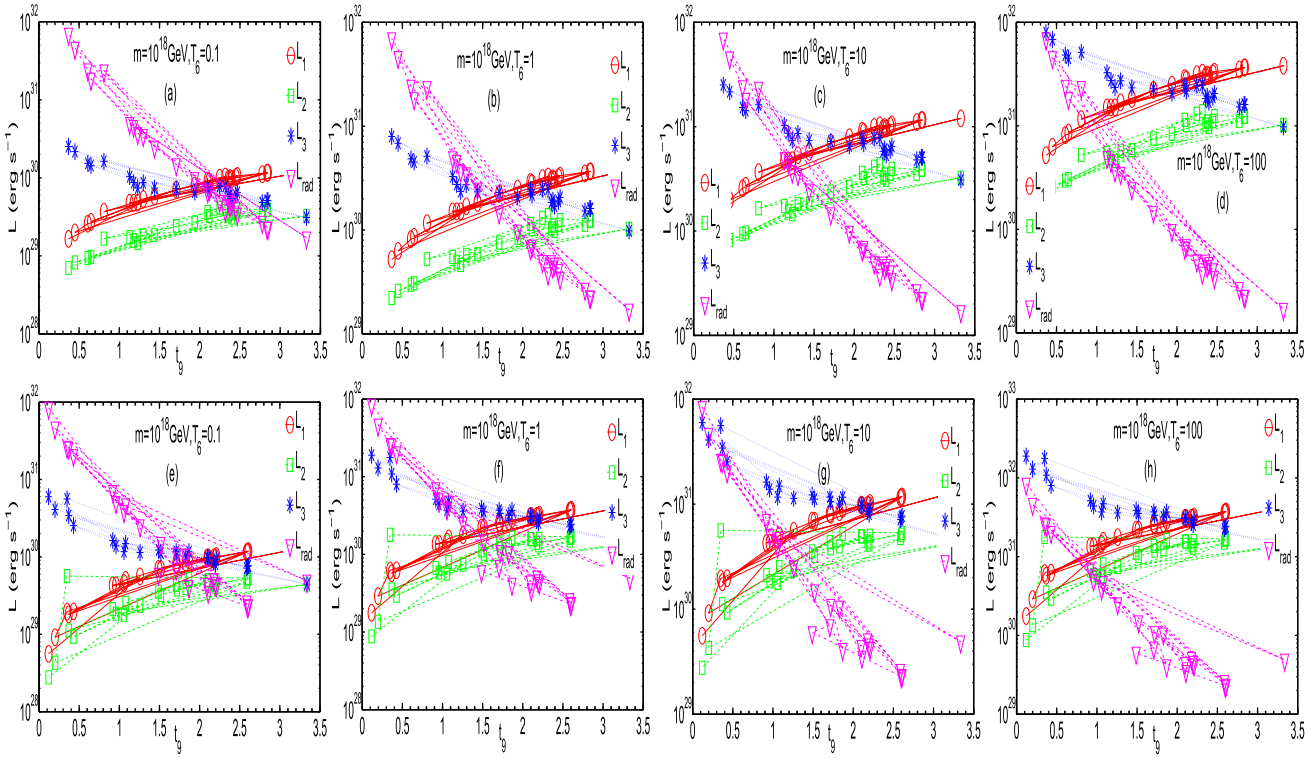

Fig. 8 The luminosities as a function of T_9 for the O+Ne (**a**–**d**) and C+O (**e**–**h**) core high mass WDs [30] when $m = 10^{18}$ GeV, and $\sigma_m = 10^{-26}$ cm^2, $\phi_m = 10^{-28}$ cm^{-2} s^{-1} sr^{-1} at the temperature of $T_6 = 0.1, 1, 10, 100$

Table 6 The comparisons among several luminosities due to RC effect of O+Ne core high mass WDs when $T_6 = 0.1$, and $\sigma_m = 10^{-26}\text{cm}^2$. Some typical astronomical conditions of CD_i (i=1, 2, 3, 4) are noted as $m = 10^{15}$ GeV, $\phi_m = 10^{-26}\,\text{cm}^{-2}\,\text{s}^{-1}\,\text{sr}^{-1}$; $m = 10^{15}$ GeV, $\phi_m = 10^{-28}\,\text{cm}^{-2}\,\text{s}^{-1}\,\text{sr}^{-1}$; $m = 10^{18}$ GeV, $\phi_m = 10^{-26}\,\text{cm}^{-2}\,\text{s}^{-1}\,\text{sr}^{-1}$; $m = 10^{18}$ GeV, $\phi_m = 10^{-28}\,\text{cm}^{-2}\,\text{s}^{-1}\,\text{sr}^{-1}$, respectively

Star	L_{rad}	CD_1			CD_2			CD_3			CD_4		
		L_1	L_2	L_3	L_1	L_2	L_3	L_1	L_2	L_3	L_1	L_2	L_3
1	2.2799e29	2.2184e30	7.4256e29	8.2292e29	2.2184e28	7.4256e27	1.5420e31	1.9966e32	6.6830e31	4.6962e28	1.9966e30	6.6830e29	8.7999e29
2	5.0029e29	1.9101e30	7.9504e29	1.2602e30	1.9101e28	7.9504e27	2.3614e31	1.7190e32	7.1554e31	7.1919e28	1.7190e30	7.1554e29	1.3476e30
3	6.6424e29	1.7537e30	6.9495e29	1.2464e30	1.7537e28	6.9495e27	2.3356e31	1.5783e32	6.2545e31	7.1132e28	1.5783e30	6.2545e29	1.3329e30
4	2.3536e31	7.0465e29	3.1780e29	2.6200e30	7.0465e27	3.1780e27	4.9094e31	6.3418e31	2.8602e31	1.4952e29	6.3418e29	2.8602e29	2.8017e30
5	2.7024e29	2.1260e30	6.8008e29	7.7710e29	2.1260e28	6.8008e27	1.4562e31	1.9134e32	6.1207e31	4.4348e28	1.9134e30	6.1207e29	8.3099e29
6	4.5818e31	3.8123e29	1.5768e29	3.4856e30	3.8123e27	1.5768e27	6.5314e31	3.4311e31	1.4192e31	1.9892e29	3.4311e29	1.4192e29	3.7273e30
7	2.4263e31	4.9380e29	1.7990e29	2.4673e30	4.9380e27	1.7990e27	4.6232e31	4.4442e31	1.6191e31	1.4080e29	4.4442e29	1.6191e29	2.6384e30
8	2.2598e29	2.2262e30	7.4517e29	8.2108e29	2.2262e28	7.4517e27	1.5386e31	2.0036e32	6.7066e31	4.6857e28	2.0036e30	6.7066e29	8.7802e29
9	4.9747e29	1.8513e30	6.2555e29	9.3897e29	1.8513e28	6.2555e27	1.7595e31	1.6661e32	5.6299e31	5.3585e28	1.6661e30	5.6299e29	1.0041e30
10	4.4181e29	1.8986e30	6.6715e29	9.8795e29	1.8986e28	6.6715e27	1.8512e31	1.7088e32	6.0043e31	5.6380e28	1.7088e30	6.0043e29	1.0565e30
11	9.8051e29	1.5186e30	5.1071e29	1.0562e30	1.5186e28	5.1071e27	1.9792e31	1.3667e32	4.5964e31	6.0276e28	1.3667e30	4.5964e29	1.1295e30
12	3.8014e29	1.9816e30	8.4088e29	1.2615e30	1.9816e28	8.4088e27	2.3638e31	1.7834e32	7.5680e31	7.1991e28	1.7834e30	7.5680e29	1.3490e30
13	3.4973e30	1.0241e30	3.4937e29	1.3918e30	1.0241e28	3.4937e27	2.6079e31	9.2167e31	3.1443e31	7.9426e28	9.2167e29	3.1443e29	1.4883e30
14	4.5720e30	9.1397e29	3.0032e29	1.3990e30	9.1397e27	3.0032e27	2.6214e31	8.2257e31	2.7029e31	7.9836e28	8.2257e29	2.7029e29	1.4960e30
15	1.7014e29	2.3097e30	6.2235e29	4.9999e29	2.3097e28	6.2235e27	9.3689e30	2.0788e32	5.6011e31	2.8533e28	2.0788e30	5.6011e29	5.3466e29
16	4.9730e30	9.1475e29	3.3325e29	1.6666e30	9.1475e27	3.3325e27	3.1229e31	8.2327e31	2.9992e31	9.5109e28	8.2327e29	2.9992e29	1.7822e30
17	3.7072e30	9.1678e29	2.7881e29	1.1983e30	9.1678e27	2.7881e27	2.2455e31	8.2510e31	2.5092e31	6.8386e28	8.2510e29	2.5092e29	1.2814e30
18	4.7162e29	1.8432e30	5.9485e29	8.6552e29	1.8432e28	5.9485e27	1.6218e31	1.6589e32	5.3536e31	4.9393e28	1.6589e30	5.3536e29	9.2554e29
19	3.4427e29	2.0204e30	7.5617e29	1.0491e30	2.0204e28	7.5617e27	1.9658e31	1.8184e32	6.8056e31	7.9426e28	1.8184e30	6.8056e29	1.1218e30
20	7.0197e29	1.7126e30	6.2062e29	1.1090e30	1.7126e28	6.2062e27	2.0780e31	1.5413e32	5.5856e31	7.9836e28	1.5413e30	5.5856e29	1.1859e30
21	4.0985e29	1.9504e30	6.8190e29	9.6312e29	1.9504e28	6.8190e27	1.8047e31	1.7554e32	6.1371e31	2.8533e28	1.7554e30	6.1371e29	1.0299e30
22	1.4729e30	1.3471e30	4.5955e29	1.1690e30	1.3471e28	4.5955e27	2.1905e31	1.2124e32	4.1360e31	9.5109e28	1.2124e30	4.1360e29	1.2500e30
23	1.8395e31	5.2180e29	1.8617e29	2.3043e30	5.2180e27	1.8617e27	4.3179e31	4.6962e31	1.6755e31	6.8386e28	4.6962e29	1.6755e29	2.4641e30
24	2.4874e30	1.1036e30	3.5458e29	1.1895e30	1.1036e28	3.5458e27	2.2289e31	9.9321e31	3.1912e31	4.9393e28	9.9321e29	3.1912e29	1.2720e30
25	6.9391e31	3.1603e29	1.3411e29	4.0574e30	3.1603e27	1.3411e27	7.6029e31	2.8443e31	1.2070e31	2.3155e29	2.8443e29	1.2070e29	4.3388e30

Table 7 The comparisons among several luminosities due to RC effect of O+Ne core high mass WDs when $T_6 = 10$, and $\sigma_m = 10^{-26}\text{cm}^2$. Some typical astronomical conditions of CD_i (i=1, 2, 3, 4) are noted as $m = 10^{15}$ GeV, $\phi_m = 10^{-26}\,\text{cm}^{-2}\,\text{s}^{-1}\,\text{sr}^{-1}$; $m = 10^{15}$ GeV, $\phi_m = 10^{-28}\,\text{cm}^{-2}\,\text{s}^{-1}\,\text{sr}^{-1}$; $m = 10^{18}$ GeV, $\phi_m = 10^{-26}\,\text{cm}^{-2}\,\text{s}^{-1}\,\text{sr}^{-1}$; $m = 10^{18}$ GeV, $\phi_m = 10^{-28}\,\text{cm}^{-2}\,\text{s}^{-1}\,\text{sr}^{-1}$, respectively

Star	L_{rad}	CD_1			CD_2			CD_3			CD_4		
		L_1	L_2	L_3	L_1	L_2	L_3	L_1	L_2	L_3	L_1	L_2	L_3
1	2.2799e29	2.2184e31	7.4255e30	8.2292e30	2.2184e29	7.4255e28	1.5420e32	1.9966e33	6.6829e32	4.6962e29	1.9966e31	6.6829e30	8.7999e30
2	5.0029e29	1.9101e31	7.9503e30	1.2602e31	1.9101e29	7.9503e28	2.3614e32	1.7190e33	7.1553e32	7.1919e29	1.7190e31	7.1553e30	1.3476e31
3	6.6424e29	1.7537e31	6.9493e30	1.2464e31	1.7537e29	6.9493e28	2.3356e32	1.5783e33	6.2544e32	7.1132e29	1.5783e31	6.2544e30	1.3329e31
4	2.3536e31	7.0465e30	3.1780e30	2.6200e31	7.0465e28	3.1780e28	4.9094e32	6.3418e32	2.8602e32	1.4952e30	6.3418e30	2.8602e30	2.8017e31
5	2.7024e29	2.1260e31	6.8007e30	7.7710e30	2.1260e29	6.8007e28	1.4562e32	1.9134e33	6.1206e32	4.4348e29	1.9134e31	6.1206e30	8.3099e30
6	4.5818e31	3.8123e30	1.5768e30	3.4856e31	3.8123e28	1.5768e28	6.5314e32	3.4311e32	1.4191e32	1.9892e30	3.4311e30	1.4191e30	3.7273e31
7	2.4263e31	4.9380e30	1.7989e30	2.4673e31	4.9380e28	1.7989e28	4.6232e32	4.4442e32	1.6190e32	1.4080e30	4.4442e30	1.6190e30	2.6384e31
8	2.2598e29	2.2262e31	7.4516e30	8.2108e30	2.2262e29	7.4516e28	1.5386e32	2.0036e33	6.7064e32	4.6857e29	2.0036e31	6.7064e30	8.7802e30
9	4.9747e29	1.8513e31	6.2553e30	9.3897e30	1.8513e29	6.2553e28	1.7595e32	1.6661e33	5.6298e32	5.3585e29	1.6661e31	5.6298e30	1.0041e31
10	4.4181e29	1.8986e31	6.6714e30	9.8795e30	1.8986e29	6.6714e28	1.8512e32	1.7088e33	6.0042e32	5.6380e29	1.7088e31	6.0042e30	1.0565e31
11	9.8051e29	1.5186e31	5.1070e30	1.0562e31	1.5186e29	5.1070e28	1.9792e32	1.3667e33	4.5963e32	6.0276e29	1.3667e31	4.5963e30	1.1295e31
12	3.8014e29	1.9816e31	8.4087e30	1.2615e31	1.9816e29	8.4087e28	2.3638e32	1.7834e33	7.5678e32	7.1991e29	1.7834e31	7.5678e30	1.3490e31
13	3.4973e30	1.0241e31	3.4936e30	1.3918e31	1.0241e29	3.4936e28	2.6079e32	9.2167e32	3.1442e32	7.9426e29	9.2167e30	3.1442e30	1.4883e31
14	4.5720e30	9.1397e30	3.0031e30	1.3990e31	9.1397e28	3.0031e28	2.6214e32	8.2257e32	2.7028e32	7.9836e29	8.2257e30	2.7028e30	1.4960e31
15	1.7014e29	2.3097e31	6.2233e30	4.9999e30	2.3097e29	6.2233e28	9.3689e31	2.0788e33	5.6010e32	2.8533e29	2.0788e31	5.6010e30	5.3466e30
16	4.9730e30	9.1475e30	3.3324e30	1.6666e31	9.1475e28	3.3324e28	3.1229e32	8.2327e32	2.9992e32	9.5109e29	8.2327e30	2.9992e30	1.7822e31
17	3.7072e30	9.1678e30	2.7880e30	1.1983e31	9.1678e28	2.7880e28	2.2455e32	8.2510e32	2.5092e32	6.8386e29	8.2501e30	2.5092e30	1.2814e31
18	4.7162e29	1.8432e31	5.9484e30	8.6552e30	1.8432e29	5.9484e28	1.6218e32	1.6589e33	5.3535e32	4.9393e29	1.6589e31	5.3535e30	9.2554e30
19	3.4427e29	2.0204e31	7.5616e30	1.0491e31	2.0204e29	7.5616e28	1.9658e32	1.8184e33	6.8054e32	5.9868e29	1.8184e31	6.8054e30	1.1218e31
20	7.0197e29	1.7126e31	6.2061e30	1.1090e31	1.7126e29	6.2061e28	2.0780e32	1.5413e33	5.5855e32	6.3285e29	1.5413e31	5.5855e30	1.1859e31
21	4.0985e29	1.9504e31	6.8189e30	9.6312e30	1.9504e29	6.8189e28	1.8047e32	1.7554e33	6.1370e32	5.4963e29	1.7554e31	6.1370e30	1.0299e31
22	1.4729e30	1.3471e31	4.5954e30	1.1690e31	1.3471e29	4.5954e28	2.1905e32	1.2124e33	4.1359e32	6.6711e29	1.2124e31	4.1359e30	1.2500e31
23	1.8395e31	5.2180e30	1.8617e30	2.3043e31	5.2180e28	1.8617e28	4.3179e32	4.6962e32	1.6755e32	1.3150e30	4.6962e30	1.6755e30	2.4641e31
24	2.4874e30	1.1036e31	3.5457e30	1.1895e31	1.1036e29	3.5457e28	2.2289e32	9.9321e32	3.1911e32	6.7882e29	9.9321e30	3.1911e30	1.2720e31
25	6.9391e31	3.1603e30	1.3410e30	4.0574e31	3.1603e28	1.3410e28	7.6029e32	2.8443e32	1.2069e32	2.3155e30	2.8443e30	1.2069e30	4.3388e31

Table 8 The comparisons among several luminosities due to RC effect of C+O core high mass WDs when $T_6 = 0.1$, and $\sigma_m = 10^{-26}\text{cm}^2$. Some typical astronomical conditions of CD_i (i=1, 2, 3, 4) are noted as $m = 10^{15}$ GeV, $\phi_m = 10^{-26}\,\text{cm}^{-2}\,\text{s}^{-1}\,\text{sr}^{-1}$; $m = 10^{15}$ GeV, $\phi_m = 10^{-28}\,\text{cm}^{-2}\,\text{s}^{-1}\,\text{sr}^{-1}$; $m = 10^{18}$ GeV, $\phi_m = 10^{-26}\,\text{cm}^{-2}\,\text{s}^{-1}\,\text{sr}^{-1}$; $m = 10^{18}$ GeV, $\phi_m = 10^{-28}\,\text{cm}^{-2}\,\text{s}^{-1}\,\text{sr}^{-1}$, respectively

star	L_{rad}	CD_1			CD_2			CD_3			CD_4		
		L_1	L_2	L_3	L_1	L_2	L_3	L_1	L_2	L_3	L_1	L_2	L_3
1	2.2935e29	2.2435e30	9.8423e29	1.2139e30	2.2435e28	9.8423e27	2.2747e31	2.0192e32	8.8581e31	6.9276e28	2.0192e30	8.8581e29	1.2981e30
2	6.0099e29	1.3387e30	6.8187e29	1.9801e30	1.3387e28	6.8187e27	3.7103e31	1.2049e32	6.1369e31	1.1300e29	1.2049e30	6.1369e29	2.1174e30
3	6.9986e29	1.5549e30	8.3329e29	1.8882e30	1.5549e28	8.3329e27	3.5381e31	1.3994e32	7.4996e31	1.0775e29	1.3994e30	7.4996e29	2.0191e30
4	2.5588e31	3.4662e29	2.1424e29	5.5244e30	3.4662e27	2.1424e27	1.0352e32	3.1196e31	1.9282e31	3.1527e29	3.1196e29	1.9282e29	5.9075e30
5	2.6327e29	2.1987e30	9.1518e29	1.1523e30	2.1987e28	9.1518e27	2.1592e31	1.9788e32	8.2366e31	6.5758e28	1.9788e30	8.2366e29	1.2322e30
6	4.6472e31	1.7576e29	8.2178e28	6.6002e30	1.7576e27	8.2178e26	1.2368e32	1.5818e31	7.3961e30	3.7666e29	1.5818e29	7.3961e28	7.0579e30
7	2.6224e31	3.7587e29	1.0820e30	9.0328e30	3.7587e27	1.0820e28	1.6926e32	3.3828e31	9.7377e31	5.1548e29	3.3828e29	9.7377e29	9.6592e30
8	2.3600e29	2.2705e30	1.0240e30	1.2443e30	2.2705e28	1.0240e28	2.3316e31	2.0435e32	9.2163e31	7.1010e28	2.0435e30	9.2163e29	1.3306e30
9	5.1389e29	1.8926e30	8.4763e29	1.3859e30	1.8926e28	8.4763e27	2.5970e31	1.7034e32	7.6286e31	7.9091e28	1.7034e30	7.6286e29	1.4820e30
10	4.4539e29	1.8830e30	9.5130e29	1.5810e30	1.8830e28	9.5130e27	2.9625e31	1.6947e32	8.5617e31	9.0225e28	1.6947e30	8.5617e29	1.6906e30
11	1.0928e30	1.5207e30	7.2717e29	1.7126e30	1.5207e28	7.2717e27	3.2092e31	1.3686e32	6.5445e31	9.7737e28	1.3686e30	6.5445e29	1.8314e30
12	4.1640e29	1.7277e30	9.9606e29	1.8811e30	1.7277e28	9.9606e27	3.5249e31	1.5549e32	8.9646e31	1.0735e29	1.5549e30	8.9646e29	2.0116e30
13	4.7418e30	9.6646e29	4.8433e29	2.3977e30	9.6646e27	4.8433e27	4.4929e31	8.6982e31	4.3589e31	1.3683e29	8.6982e29	4.3589e29	2.5640e30
14	5.0741e30	8.2333e29	3.5399e29	2.2422e30	8.2333e27	3.5399e27	4.2015e31	7.4100e31	3.1859e31	1.2796e29	7.4100e29	3.1859e29	2.3977e30
15	4.9030e29	2.5815e30	8.4441e29	7.1644e29	2.5815e28	8.4441e27	1.3425e31	2.3234e32	7.5997e31	4.0886e28	2.3234e30	7.5997e29	7.6613e29
16	7.0447e30	8.1998e29	4.0442e29	2.6199e30	8.1998e27	4.0442e27	4.9092e31	7.3798e31	3.6398e31	1.4951e29	7.3798e29	3.6398e29	2.8016e30
17	3.8962e30	8.7972e29	3.4253e29	1.8864e30	8.7972e27	3.4253e27	3.5348e31	7.9175e31	3.0828e31	1.0765e29	7.9175e29	3.0828e29	2.0172e30
18	4.5949e29	1.8753e30	7.9062e29	1.2960e30	1.8753e28	7.9062e27	2.4284e31	1.6877e32	7.1156e31	7.3959e28	1.6877e30	7.1156e29	1.3859e30
19	3.5160e29	1.8882e30	9.4623e29	1.5657e30	1.8882e28	9.4623e27	2.9338e31	1.6994e32	8.5161e31	8.9351e28	1.6994e30	8.5161e29	1.6743e30
20	1.0523e30	1.6114e30	7.5906e29	1.6243e30	1.6114e28	7.5906e27	3.0437e31	1.4503e32	6.8315e31	9.2698e28	1.4503e30	6.8315e29	1.7370e30
21	4.2674e29	1.9658e30	9.6196e29	1.4899e30	1.9658e28	9.6196e27	2.7918e31	1.7692e32	8.6576e31	8.5026e28	1.7692e30	8.6576e29	1.5932e30
22	1.5028e30	1.3331e30	6.1873e29	1.8035e30	1.3331e28	6.1873e27	3.3794e31	1.1998e32	5.5686e31	1.0292e29	1.1998e30	5.5686e29	1.9285e30
23	2.0451e31	3.7865e29	1.7836e29	4.0826e30	3.7865e27	1.7836e27	7.6501e31	3.4078e31	1.6052e31	2.3299e29	3.4078e29	1.6052e29	4.3657e30
24	2.5375e30	1.0718e30	4.4899e29	1.8351e30	1.0718e28	4.4899e27	3.4387e31	9.6464e31	4.0409e31	1.0473e29	9.6464e29	4.0409e29	1.9624e30
25	8.3758e31	1.0717e29	5.3278e28	9.6412e30	1.0717e27	5.3278e26	1.8066e32	9.6452e30	4.7950e30	5.5020e29	9.6452e28	4.7950e28	1.0310e31

Table 9 The comparisons among several luminosities due to RC effect of C+O core high mass WDs when $T_6 = 10$, and $\sigma_m = 10^{26}\text{cm}^2$. Some typical astronomical conditions of CD_i (i=1, 2, 3, 4) are noted as $m = 10^{15}$ GeV, $\phi_m = 10^{-26}\,\text{cm}^{-2}\,\text{s}^{-1}\,\text{sr}^{-1}$; $m = 10^{15}$ GeV, $\phi_m = 10^{-28}\,\text{cm}^{-2}\,\text{s}^{-1}\,\text{sr}^{-1}$; $m = 10^{18}$ GeV, $\phi_m = 10^{-26}\,\text{cm}^{-2}\,\text{s}^{-1}\,\text{sr}^{-1}$; $m = 10^{18}$ GeV, $\phi_m = 10^{-28}\,\text{cm}^{-2}\,\text{s}^{-1}\,\text{sr}^{-1}$, respectively

star	L_{rad}	CD_1			CD_2			CD_3			CD_4		
		L_1	L_2	L_3	L_1	L_2	L_3	L_1	L_2	L_3	L_1	L_2	L_3
1	2.2935e29	2.2435e31	9.8423e30	1.2139e31	2.2435e29	9.8423e28	2.2747e32	2.0192e33	8.8581e32	6.9276e29	2.0192e31	8.8581e30	1.2981e31
2	6.0099e29	1.3387e31	6.8187e30	1.9801e31	1.3387e29	6.8187e28	3.7103e32	1.2049e33	6.1369e32	1.1300e30	1.2049e31	6.1369e30	2.1174e31
3	6.9986e29	1.5549e31	8.3329e30	1.8882e31	1.5549e29	8.3329e28	3.5381e32	1.3994e33	7.4996e32	1.0775e30	1.3994e31	7.4996e30	2.0191e31
4	2.5588e31	3.4662e30	2.1424e30	5.5244e31	3.4662e28	2.1424e28	1.0352e33	3.1196e32	1.9282e32	3.1527e30	3.1196e30	1.9282e30	5.9075e31
5	2.6327e29	2.1987e31	9.1518e30	1.1523e31	2.1987e29	9.1518e28	2.1592e32	1.9788e33	8.2366e32	6.5758e29	1.9788e31	8.2366e30	1.2322e31
6	4.6472e31	1.7576e30	8.2178e29	6.6002e31	1.7576e28	8.2178e27	1.2368e33	1.5818e32	7.3961e31	3.7666e30	1.5818e30	7.3961e29	7.0579e31
7	2.6224e31	3.7587e30	1.0820e31	9.0328e31	3.7587e28	1.0820e29	1.6926e33	3.3828e32	9.7377e32	5.1548e30	3.3828e30	9.7377e30	9.6592e31
8	2.3600e29	2.2705e31	1.0240e31	1.2443e31	2.2705e29	1.0240e29	2.3316e32	2.0435e33	9.2163e32	7.1010e29	2.0435e31	9.2163e30	1.3306e31
9	5.1389e29	1.8926e31	8.4763e30	1.3859e31	1.8926e29	8.4763e28	2.5970e32	1.7034e33	7.6286e32	7.9091e29	1.7034e31	7.6286e30	1.4820e31
10	4.4539e29	1.8830e31	9.5130e30	1.5810e31	1.8830e29	9.5130e28	2.9625e32	1.6947e33	8.5617e32	9.0225e29	1.6947e31	8.5617e30	1.6906e31
11	1.0928e30	1.5207e31	7.2717e30	1.7126e31	1.5207e29	7.2717e28	3.2092e32	1.3686e33	6.5445e32	9.7737e29	1.3686e31	6.5445e30	1.8314e31
12	4.1640e29	1.7277e31	9.9606e30	1.8811e31	1.7277e29	9.9606e28	3.5249e32	1.5549e33	8.9646e32	1.0735e30	1.5549e31	8.9646e30	2.0116e31
13	4.7418e30	9.6646e30	4.8433e30	2.3977e31	9.6646e28	4.8433e28	4.4929e32	8.6982e32	4.3589e32	1.3683e30	8.6982e30	4.3589e30	2.5640e31
14	5.0741e30	8.2333e30	3.5399e30	2.2422e31	8.2333e28	3.5399e28	4.2015e32	7.4100e32	3.1859e32	1.2796e30	7.4100e30	3.1859e30	2.3977e31
15	4.9030e29	2.5815e31	8.4441e30	7.1644e30	2.5815e29	8.4441e28	1.3425e32	2.3234e33	7.5997e32	4.0886e29	2.3234e31	7.5997e30	7.6613e30
16	7.0447e30	8.1998e30	4.0442e29	2.6199e31	8.1998e28	4.0442e28	4.9092e32	7.3798e32	3.6398e32	1.4951e30	7.3798e30	3.6398e30	2.8016e31
17	3.8962e30	8.7972e30	3.4253e29	1.8864e31	8.7972e28	3.4253e28	3.5348e32	7.9175e32	3.0828e32	1.0765e30	7.9175e30	3.0828e30	2.0172e31
18	4.5949e29	1.8753e31	7.9062e29	1.2960e31	1.8753e29	7.9062e28	2.4284e32	1.6877e33	7.1156e32	7.3959e29	1.6877e31	7.1156e30	1.3859e31
19	3.5160e29	1.8882e31	9.4623e29	1.5657e31	1.8882e29	9.4623e28	2.9338e32	1.6994e33	8.5161e32	8.9351e29	1.6994e31	8.5161e30	1.6743e31
20	1.0523e30	1.6114e31	7.5906e29	1.6243e31	1.6114e29	7.5906e28	3.0437e32	1.4503e33	6.8315e32	9.2698e29	1.4503e31	6.8315e30	1.7370e31
21	4.2674e29	1.9658e31	9.6196e29	1.4899e31	1.9658e29	9.6196e28	2.7918e32	1.7692e33	8.6576e32	8.5026e29	1.7692e31	8.6576e30	1.5932e31
22	1.5028e30	1.3331e31	6.1873e29	1.8035e31	1.3331e29	6.1873e28	3.3794e32	1.1998e33	5.5686e32	1.0292e30	1.1998e31	5.5686e30	1.9285e31
23	2.0451e31	3.7865e30	1.7836e29	4.0826e31	3.7865e28	1.7836e28	7.6501e32	3.4078e32	1.6052e32	2.3299e30	3.4078e30	1.6052e30	4.3657e31
24	2.5375e30	1.0718e31	4.4899e29	1.8351e31	1.0718e29	4.4899e28	3.4387e32	9.6464e32	4.0409e32	1.0473e30	9.6464e30	4.0409e30	1.9624e31
25	8.3758e31	1.0717e30	5.3278e28	9.6412e31	1.0717e28	5.3278e27	1.8066e33	9.6452e31	4.7950e31	5.5020e30	9.6452e29	4.7950e29	1.0310e32

that the bound has been stated as $\phi_m(\sigma v)_{-28} < 1.3 \times 10^{-20}(v/(10^{-3}c)^2)\text{cm}^{-2}\,\text{s}^{-1}\,\text{sr}^{-1}$. If the mass of MM is 10^{17} GeV, $\beta = 10^{-3}$, and $\sigma_m = 10^{-26}\text{cm}^2$, we can obtain $\phi_m < 4.33 \times 10^{-26}\,\text{cm}^{-2}\,\text{sr}^{-1}\,\text{s}^{-1}$.

Tables 4 and 5 show the comparisons of the upper limits of the MMs flux ϕ_m with those of [10] of WD-1136-286 when $\sigma = 10^{-26}\text{cm}^2$. Our upper limits of the MMs flux can be 5, 7 orders of magnitude higher than those of [10] for model (II, III), respectively, but can be 2 orders of magnitude lower for model (II).

Tables 10 and 11 show our results obtained on the upper limits of the MMs flux ϕ_m by $L_{\text{rad}} = L_{(1,2,3)}$ for three model (I, II, III) due to RC effect for O+Ne, and C+O core high mass WDs samples [30] when $\sigma_m = 10^{-26}\text{cm}^2$, respectively. One can conclude that when other parameters are certain, as the temperature increases, the upper limits of the MMs flux decreases. For example, the MMs flux ϕ_m decreases from 8.6838×10^{-26} to 2.7461×10^{-26}, then decrease from 8.6838×10^{-27} to 2.7461×10^{-27} for model (I) when $\beta = 10^{-4}$, T_6 increases from 0.1 to 100 in Table 11. It is easy to understand for this changes due to the MMs flux $\phi_m \propto T^{-1/2}$ according to Eqs. (1, 6, 18, 19, 22). The upper limits of the MMs flux ϕ_m, on the other hand, increases as the β increases. For instance, for model (I), the upper limits of the MMs flux ϕ_m increases from 2.4397×10^{-26} to 7.0399×10^{-20} when the β changes from 10^{-4} to 0.90 at $T_6 = 0.1$ in Table 10.

From Table 10, when $10^{-4} \leq \beta \leq 10^{-2}$, we find that the maximum of the upper limits of the MMs flux ϕ_m can be 2.4397×10^{-24}, 9.1989×10^{-19}, and 1.9203×10^{-23} for model (I, II, III), respectively. On the other hand, when $0.1 \leq \beta \leq 0.995$, the maximum of the upper limits of the MMs flux ϕ_m can be 2.4153×10^{-20}, 9.1071×10^{-15}, and 1.8816×10^{-19} for model (I, II, III), respectively. Table 11 also shows that the maximum of the upper limits of the MMs flux ϕ_m can be 8.6838×10^{-24}, 2.7949×10^{-18}, and 3.4684×10^{-23} when $10^{-4} \leq \beta \leq 10^{-2}$ for model (I, II, III), respectively. However, when $0.1 \leq \beta \leq 0.995$, the maximum of the upper limits of the MMs flux ϕ_m can be 8.5972×10^{-20}, 2.7670×10^{-14}, and 3.4338×10^{-19} for model (I, II, III), respectively.

It is all known that three classes for the astrophysical MMs flux bounds are given as follows. Firstly, either locally or in the Universe, the bounds will base on the mass density of MMs. Secondly, in neutron stars and WDs, the bounds will base on monopole catalysis of nucleon decay. Finally, bounds base on the monopole energy drain from astrophysical magnetic fields. However, it is very stringent for the flux limits, which bases upon MM's catalysis of nucleon decay. Due to RC effect, each decay can release about 1GeV energy causing the star (e.g., WDs, and neutron star) to heat up and radiate large amounts of energy with the form of neutrino or the X-rays. For example, from observed limits on the x-ray flux from neutron stars, a bound was placed on the product

Table 10 The maximum value of the upper limits of the MMs flux ϕ_m obtained by $L_{\text{rad}} = L_{(1,2,3)}$ of three MMs model (I, II, III) due to RC effect for 25 O+Ne core high mass white dwarf samples [30] when $\sigma_m = 10^{-26}\text{cm}^2$

β	m	$T_6 = 0.1$			$T_6 = 1$			$T_6 = 10$			$T_6 = 100$		
		I	II	III	I	II	III	I	II	III	I	II	III
10^{-4}	9.00e18	2.4397e−26	9.1989e−21	8.4385e−28	7.7149e−27	2.9089e−21	5.1520e−27	2.4397e−27	9.1990e−22	3.1455e−26	7.7149e−28	2.9144e−22	1.9205e−25
10^{-3}	9.00e16	2.4397e−26	9.1989e−21	8.4385e−28	7.7149e−27	2.9089e−21	5.1520e−27	2.4397e−27	9.1990e−22	3.1455e−26	7.7149e−28	2.9144e−22	1.9205e−25
10^{-2}	9.00e14	2.4397e−24	9.1989e−19	8.4385e−26	7.7149e−25	2.9089e−19	5.1520e−25	2.4397e−25	9.1990e−20	3.1455e−24	7.7149e−26	2.9144e−20	1.9205e−23
0.1	9.00e12	2.4397e−22	9.1989e−17	8.4385e−24	7.7149e−23	2.9089e−17	5.1520e−23	2.4397e−23	9.1990e−18	3.1455e−22	7.7149e−24	2.9144e−18	1.9205e−21
0.2	2.25e12	9.7586e−22	3.6795e−16	3.3754e−23	3.0859e−22	1.1636e−16	2.0608e−22	9.7586e−23	3.6796e−17	1.2582e−21	3.0859e−23	1.1658e−17	7.6819e−21
0.3	1.00e12	2.1957e−21	8.2790e−16	7.5946e−23	6.9434e−22	2.6180e−16	4.6368e−22	2.1957e−22	8.2791e−17	2.8310e−21	6.9434e−23	2.6230e−17	1.7284e−20
0.4	5.625e11	3.9034e−21	1.4718e−15	1.3502e−22	1.2344e−21	4.6543e−16	8.2433e−22	3.9034e−22	1.4718e−16	5.0328e−21	1.2344e−22	4.6630e−17	3.0728e−20
0.5	3.60e11	6.0991e−21	2.2997e−15	2.1096e−22	1.9287e−21	7.2723e−16	1.2880e−21	6.0991e−22	2.2998e−16	7.8638e−21	1.9287e−22	7.2860e−17	4.8012e−20
0.6	2.50e11	8.7827e−21	3.3116e−15	3.0379e−22	2.7773e−21	1.0472e−15	1.8547e−21	8.7827e−22	3.3117e−16	1.1324e−20	2.7773e−22	1.0492e−16	6.9137e−20
0.7	1.84e11	1.1954e−20	4.5074e−15	4.1349e−22	3.7803e−21	1.4254e−15	2.5245e−21	1.1954e−21	4.5075e−16	1.5413e−20	3.7803e−22	1.4281e−16	9.4103e−20
0.8	1.42e11	1.5614e−20	5.8873e−15	5.4006e−22	4.9375e−21	1.8617e−15	3.2973e−21	1.5614e−21	5.8874e−16	2.0131e−20	4.9375e−22	1.8652e−16	1.2291e−19
0.9	1.11e11	1.9761e−20	7.4511e−15	6.8352v22	6.2490e−21	2.3562e−15	4.1732e−21	1.9761e−21	7.4512e−16	2.5479e−20	6.2490e−22	2.3607e−16	1.5556e−19
0.995	9.00e10	2.4153e−20	9.1071e−15	8.2678e−22	7.6379e−21	2.8799e−15	5.0478e−21	2.4153e−21	9.1073e−16	3.0819e−20	7.6379e−22	2.8853e−16	1.8816e−19

Table 11 The maximum value of the upper limits of the MMs flux ϕ_m obtained by $L_{\rm rad} = L_{(1,2,3)}$ of three MMs model (I, II, III) due to RC effect for 25 C+O core high mass white dwarf samples [30] when $\sigma_m = 10^{-26}{\rm cm}^2$

β	m	$T_6 = 0.1$			$T_6 = 1$			$T_6 = 10$			$T_6 = 100$		
		I	II	III	I	II	III	I	II	III	I	II	III
10^{-4}	9.00e18	8.6838e−26	2.7949e−20	1.5240e−27	2.7461e−26	8.8382e−21	9.3046e−27	8.6838e−27	2.7949e−21	5.6808e−26	2.7461e−27	8.8548e−22	3.4684e−25
10^{-3}	9.00e16	8.6838e−26	2.7949e−20	1.5240e−27	2.7461e−26	8.8382e−21	9.3046e−27	8.6838e−27	2.7949e−21	5.6808e−26	2.7461e−27	8.8548e−22	3.4684e−25
10^{-2}	9.00e14	8.6838e−24	2.7949e−18	1.5240e−25	2.7461e−24	8.8382e−19	9.3046e−25	8.6838e−25	2.7949e−19	5.6808e−24	2.7461e−25	8.8548e−20	3.4684e−23
0.1	9.00e12	8.6838e−22	2.7949e−16	1.5240e−23	2.7461e−22	8.8382e−17	9.3046e−23	8.6838e−23	2.7949e−17	5.6808e−22	2.7461e−23	8.8548e−18	3.4684e−21
0.2	2.25e12	3.4735e−21	1.1180e−15	6.0960e−23	1.0984e−21	3.5353e−16	3.7218e−22	3.4735e−22	1.1180e−16	2.2723e−21	1.0984e−22	3.5419e−17	1.3874e−20
0.3	1.00e12	7.8154e−21	2.5154e−15	1.3716e−22	2.4715e−21	7.9544e−16	8.3742e−22	7.8154e−22	2.5154e−16	5.1128e−21	2.4715e−22	7.9693e−17	3.1215e−20
0.4	5.625e11	1.3894e−20	4.4718e−15	2.4384e−22	4.3937e−21	1.4141e−15	1.4887e−21	1.3894e−21	4.4719e−16	9.0894e−21	4.3937e−22	1.4168e−16	5.5494e−20
0.5	3.60e11	2.1710e−20	6.9872e−15	3.8100e−22	6.8652e−21	2.2095e−15	2.3262e−21	2.1710e−21	6.9873e−16	1.4202e−20	6.8652e−22	2.2137e−16	8.6710e−20
0.6	2.50e11	3.1262e−20	1.0062e−14	5.4864e−22	9.8858e−21	3.1818e−15	3.3497e−21	3.1262e−21	1.0062e−15	2.0451e−20	9.8858e−22	3.1877e−16	1.2486e−19
0.7	1.84e11	4.2551e−20	1.3695e−14	7.4676e−22	1.3456e−20	4.3307e−15	4.5593e−21	4.2551e−21	1.3695e−15	2.7836e−20	1.3456e−21	4.3388e−16	1.6995e−19
0.8	1.42e11	5.5577e−20	1.7887e−14	9.7536e−22	1.7575e−20	5.6564e−15	5.9550e−21	5.5577e−21	1.7888e−15	3.6357e−20	1.7575e−21	5.6671e−16	2.2198e−19
0.9	1.11e11	7.0339e−20	2.2639e−14	1.2344e−21	2.2243e−20	7.1589e−15	7.5367e−21	7.0339e−21	2.2639e−15	4.6015e−20	2.2243e−21	7.1724e−16	2.8094e−19
0.995	9.00e10	8.5972e−20	2.7670e−14	1.5088e−21	2.7187e−20	8.7500e−15	9.2118e−21	8.5972e−21	2.7671e−15	5.6242e−20	2.7187e−21	8.7665e−16	3.4338e−19

of the galactic flux of massive MMs and the cross section for monopole-catalyzed nucleon decay [53].

From Table 10, our upper limits of the MMs flux for O+Ne core mass WDs can be 2.4397×10^{-22}, 9.1989×10^{-17}, and 1.9025×10^{-21} when $10^{-4} \leq \beta \leq 0.1$ for model (I, II, III), respectively. Our results are lower about 6, 1, 5 orders of magnitude than those of [51] for model (I, II, III), respectively. However, ours are about 7, 2, 5 orders of magnitude lower than those of [52] for model (I, II, III), respectively. Our upper limits of the MMs flux, on the other hand, can be 2.4397×10^{-26}, 9.1989×10^{-21}, and 1.9025×10^{-25} when $\beta = 10^{-3}$ for model (I, II, III), respectively. Our results for model (I, II) are agreed well with those of [10], but about 5 orders of magnitude higher than those of [10] for model (III).

For C+O core mass WDs, from Table 11, our upper limits of the MMs flux can be 8.6838×10^{-22}, 2.7949×10^{-16}, and 3.4684×10^{-21} when $10^{-4} \leq \beta \leq 0.1$ for model (I, II, III), respectively. Our results are agreed well with [51] for model (II), but are lower about 6, and 5 orders of magnitude than those of [51] for model (I, III), respectively. However, ours are lower about 10, 4, 9 orders of magnitude than those of [52] for model (I, II, III), respectively. From Table 11, our upper limits of the MMs flux, on the other hand, can be 8.6838×10^{-26}, 2.7949×10^{-20}, and 3.4684×10^{-25} when $\beta = 10^{-3}$ for model (I, II, III), respectively. ours for model (I, II) are agreed well with those of [10], but about 4 orders of magnitude higher than those of [10] for model (III).

Table 12 shows that the comparisons of the upper limits of the MMs flux ϕ_m due to RC effect for our results(ϕ_{m1}, and ϕ_{m2} are corresponding to the O+Ne and C+O core mass WDs) with those of [54] (ϕ_m(Abb)), [55] (ϕ_m(Aar)$Ic40$, ϕ_m(Aar)Ic86), and [56] (ϕ_m(Alb)). Our results are about one and two orders of magnitude higher than those of [54] ([56]) for O+Ne, and C+O core mass WDs, respectively, and can be about three and four orders of magnitude higher than those of [55] (ϕ_m(Aar)$Ic40$, ϕ_m(Aar)Ic86), respectively.

Based on the above analysis, one can conclude that with the increasing of the number of MMs captured by WDs, the luminosity of MM catalyzed nuclear decay increases linearly with time until it becomes the main contribution to the total luminosity. Even one can observe that for some of the oldest WDs, the luminosity may have passed its minimum, and some reheating may have occurred.

It may be worried that the annihilation of MMs and anti-MMs could result in a significant reduction in the number of MMs and the catalytic luminosity of the monopole in the WDs. Dicus et al. [57] calculated the annihilation cross sections of MM and anti-MM caused by two-body and three-body recombination. Their results showed that this kind of annihilation has little effect on the flux and luminosity. On the other hand, some WDs nay have magnetic fields of up to 10^5G by observations. The forces generated by the magnetic field inside the WD must balance the gravitational and

Table 12 The comparisons of the upper limits of the MMs flux ϕ_m due to RC effect for our results(ϕ_{m1}, and ϕ_{m2} are corresponding to the O+Ne and C+O core mass WDs) with those of [54](ϕ_m(Abb)), [55](ϕ_m(Aar)$Ic40$, ϕ_m(Aar)Ic86), and [56](ϕ_m(Alb)). Scaling factor $n_i (i = 1 \sim 8)$ are defined as $n_i = \phi_{m1}/\phi_{mj} (i = 1 \sim 4)$, and $n_i = \phi_{m2}/\phi_{mj} (i = 5 \sim 8)$, respectively ($j = 1, 2, 3, 4$ are corresponding to the results of ϕ_m(Abb), ϕ_m(Aar)$Ic40$, ϕ_m(Aar)Ic86, and ϕ_m(Alb))

β	ϕ_m(Abb)	ϕ_m(Aar)$Ic40$	ϕ_m(Aar)Ic86	ϕ_m(Alb)	ϕ_{m1}	ϕ_{m2}	n_1	n_2	n_3	n_4	n_5	n_6	n_7	n_8
$0.500 \sim 0.599$	–	–	8.71e−18	5.90e−16	3.3006e−15	1.0028e−14	–	–	378.94	5.5942	–	–	1151.3	16.997
$0.600 \sim 0.699$	–	–	1.80e−18	3.60e−17	4.4946e−15	1.3656e−14	–	–	2497	124.85	–	–	7586.7	379.33
$0.700 \sim 0.799$	8.80e−16	7.73e−18	3.39e−18	9.10e−16	5.8726e−15	1.7843e−14	6.6734	759.72	1732.3	6.4534	20.276	2308.3	5263.4	19.608
$0.800 \sim 0.899$	1.75e−15	3.89e−18	1.039e−17	4.90e−16	7.4345e−15	2.2588e−14	4.2483	1911.2	715.54	15.172	12.907	5806.7	2174	46.098
$0.900 \sim 0.995$	2.90e−16	3.06e−18	–	2.50e−16	9.1071e−15	2.7670e−14	31.404	2976.2	–	36.428	95.414	9042.5	–	110.68

Coulomb interactions. The magnetic field may keep the MM and anti-MM distributions far enough apart for annihilation to be negligible.

Based on the above analysis, due to neglect the affect on the mass radius relation by the number of the MMs captured in WDs, and only the mass radius relation and RC effect are considered in model (I), the luminosities can be over estimated to compare to model(II) and (III) (see Eqs. (18, 22)). Pei et al. [46] investigated the highly accurate mass–radius relation of the WDs from zero to finite temperature. He estimated the temperature effect on mass–radius relation by using statistical mechanics (see Eq. (23)). According to Eq. (23) and RC effect, we discuss the number of MMs captured and the luminosities of WDs. We find the results from model (II) can be higher than the estimations from model (III) due to the effect of temperature. By considering the affect on the mass radius relationship by the number of the MMs captured in WDs (see Eqs. (35, 39)), and RC effect, one sees that the calculations in the model (III) are agreed well with the observations and may be an improving estimation than model (I) and (II).

According to our above calculations, one can see that the MM passes through the Milky Way and loses enough energy to be captured by the WDs. Monopole trapped inside a WD can catalyze the decay of nuclei. This process can be used as an energy source to keep the WD hot.

6 Conclusions and outlooks

Basing on the MMs catalytic nuclear decay, we present three MMs models of energy resource in WDs. We discuss the luminosity and compare it for our models with the observations to apply to 25 super-massive WDs. Firstly, we find that $N_2 > N_1 > N_3$ on the same astronomical condition (e.g. CD_1). The maxnium of the number of MMs captured can be 9.6943×10^{11}, and 9.0671×10^{11} for O+Ne core high mass WD J055631.17+130639.78, and C+O core high mass WD J055631.17+130639.78, respectively. Secondly, the luminosities for model (III) are agreed well with the observations and the differences are no more than one order of magnitude, but can be 2–3 orders of magnitude higher than observations for model (I), and (II). Finally, the maxnium of the upper limit of the MMs flux ϕ_m due to RC effect can be 9.1071×10^{-15}, and 2.7670×10^{-14} for O+Ne and C+O core high mass WD, respectively. Our results are about one and two orders of magnitude higher than those of [54] ([56]) for O+Ne, and C+O core mass WDs, respectively, and can be about three and four orders of magnitude higher than those of [55] (ϕ_m(Aar)$Ic40$, ϕ_m(Aar)Ic86), respectively. Based on the above analysis and discussion, the monopole-catalyzed nucleon decay process could be preventing WDs from cooling down into a stellar graveyard by keeping them hot.

In this paper, we mainly focus on MMs catalytic nuclear decay and discuss the problem on the energy resource in WDs. We obtain a new upper limits of the MM flux for the supermassive WDs. Our woks on the calculations of MM capture, the luminosity, and upper limits of the MM flux in WDs, are following the works of Refs. [10,33]. However, there may be another very interesting method to discuss the problem of monopole capture and related issues on WDs following the works of Refs. [58–62].

Through the process of the capture and subsequent annihilation, dark matter may be discovered in stars. It is usually assumed that dark matter is captured after a single scattering event in the star. However, heavy dark matter can require multiple collisions with the star to lose enough kinetic energy to become captured. If captured by the gravitational field of stars or other compact objects, dark matter can self-annihilate and produce a potentially detectable particle flux. For superheavy dark matter (e.g., MM), a large number of scattering events with nuclei inside stars are necessary to slow down the dark matter particles (e.g., MM) below the escape velocity of the stars, at which point the Dark Matter particle becomes trapped, or captured. These problems on the capture of the dark matter particle (e.g., MM) and related issues will be very interesting and challenging woks to study for us. On the other hand, the researches on MMs have always been a hot and frontier topics in the fields of nuclear physics and astrophysics. The search of MMs is still a difficult and challenging problem, and the flux of magnetic single stage in the universe is still uncertain. The neutrino emissivity rates due to RC effect also may play a key role in the process of WDS and neutron star evolution. These challenging problems will be our future issues.

Acknowledgements We would like to thank the anonymous reviewer who put forward many constructive revision suggestions for improving our paper. This work was supported in part by the National Natural Science Foundation of China under Grants 11965010, 11565020, and the Natural Science Foundation of Hainan Province of China under Grant 2019RC239, 118MS071, 114012, and the Counterpart Foundation of Sanya under Grant 2016PT43, 2019PT76, the Special Foundation of Science and Technology Cooperation for Advanced Academy and Regional of Sanya under Grant 2016YD28, the Scientific Research Starting Foundation for 515 Talented Project of Hainan Tropical Ocean University under Grant RHDRC201701.

Data Availability Statement This manuscript has no associated data or the data will not be deposited. [Authors' comment: The data that support the plots within this paper and other findings of this study are available from the corresponding author upon reasonable request].

Open Access This article is licensed under a Creative Commons Attribution 4.0 International License, which permits use, sharing, adaptation, distribution and reproduction in any medium or format, as long as you give appropriate credit to the original author(s) and the source, provide a link to the Creative Commons licence, and indicate if changes were made. The images or other third party material in this article are included in the article's Creative Commons licence, unless indicated otherwise in a credit line to the material. If material is not included in the article's Creative Commons licence and your intended use is not permitted by statutory regulation or exceeds the permitted use, you will need to obtain permission directly from the copyright holder. To view a copy of this licence, visit http://creativecommons.org/licenses/by/4.0/.
Funded by SCOAP[3].

References

1. L. Mestel, On the theory of white dwarf stars. I. The energy sources of white dwarfs. MNRAS **112**, 583 (1952)
2. L. Bildsten, D.M. Hall, Gravitational settling of 22NE in liquid white dwarf interiors. ApJL **549**, 219 (2001)
3. R.M. Avakian, The configurations of hot white dwarfs with nuclear sources of energy. CoBAO **44**, 115 (1972)
4. C.J. Deloye, L. Bildsten, Gravitational settling of ^{22}Ne in liquid white dwarf interiors: cooling and seismological effects. ApJ **580**, 1077 (2002)
5. E. Garca-Berro, L.G. Althaus, A.H. Córsico et al., Gravitational settling of 22Ne and white dwarf evolution. ApJ **677**, 473 (2008)
6. R.V. Lobato, M. Malheiro, J.G. Coelho, SGRs/AXPs as white dwarf pulsars: sources of ultra-high energetic photons with $E \sim 10^{21}$ eV. Mgm. Conf. **4313**, 4318 (2018)
7. S.H. Cheng, J.D. Cummings, B. Mnard, A cooling anomaly of high-mass white dwarfs. ApJ **886**, 100 (2019)
8. M.E. Caplan, C.J. Horowitz, A. Cumming, Neon cluster formation and phase separation during white dwarf cooling. ApJL **902L**, 44C (2020)
9. K. Freese, Do monopoles keep white dwarfs hot? ApJ **286**, 216 (1984)
10. K. Freese, E. Krasteva, Bound on the flux of magnetic monopoles from catalysis of nucleon decay in white dwarfs. PhRvD **59**, 063007 (1999)
11. C. Callan et al., Monopole catalysis of baryon decay. Nucl. Phys. **212**, 391 (1983)
12. V. Rubakov, Superheavy magnetic monopoles and decay of the proton. JETP Lett. **33**, 644 (1981)
13. M. Detrixhe, D. Besson, P.W. Gorham et al., Ultrarelativistic magnetic monopole search with the ANITA-II balloon-borne radio interferomete. PhRvD **94**, 082002 (2016)
14. M. Frank, A. Antoshkin, C. Dukes et al., Subluminal magnetic monopole search with NOvA. ICRC **36**, 888 (2019)
15. T. Fujii, A.C. Pierre, Subluminal magnetic monopole search with NOvA. ICRC **34**, 319 (2015)
16. B. Kain, Are gravitating magnetic monopoles stable? PhRvD **100**, 3003 (2019)
17. A. Rajantie, Magnetic monopoles in field theory and cosmologyr. RSPTA **370**, 5705 (2012)
18. Z.Q. Ma, J.F. Tang, Scattering of fermions on the SU(5) colorless magnetic monopole. PhLB **153**, 59 (1983)
19. J.J. Liu, Electron capture of strongly screening nuclides ^{56}Fe, ^{56}Co, ^{56}Ni, ^{56}Mn, ^{56}Cr and ^{56}V in pre-supernovae. MNRAS **433**, 1108 (2013)
20. J.J. Liu, Electron capture of iron-group nuclei in magnetars. MNRAS **438**, 930 (2014)
21. J.J. Liu, W.M. Gu, A new insight into neutrino energy loss by electron capture of iron group nuclei in magnetar surfaces. ApJS **224**, 29 (2016)
22. J.J. Liu et al., Strongly screening electron capture for nuclides ^{52,53,59,60}Fe by the shell-model Monte Carlo method in pre-supernovae. ChPhC **41**, 5101 (2017)
23. J.J. Liu, Magnetar crust electron capture for ^{55}Co and ^{56}Ni. EPJC **78**, 84 (2018)

24. Q.H. Peng, J.J. Liu, C.K. Chou, A magnetic-monopole-based mechanism to the formation of the hot big bang modeled universe. MPLA **35**, 2050030 (2020)
25. Q.H. Peng, J.J. Liu, Z.Q. Ma, Some new possible anticipated signals for existence of magnetic monopolesr. NewA **57**, 59 (2017)
26. Z.F. Gao, X.D. Li, N. Wang et al., Constraining the braking indices of magnetars. MNRAS **456**, 55 (2016)
27. Z.F. Gao, N. Wang, H. Shan et al., The dipole magnetic field and spin-down evolutions of the high braking index pulsar PSR J1640–4631. ApJ **849**, 19 (2017)
28. Z.F. Gao, N. Omar, X.C. Shi et al., The Ohmic decay of dipolar toroidal magnetic fields of magnetars. AN **340**, 1030 (2019)
29. L.Z. Deng, X.D. Li, Z.F. Gao et al., Evolution of LMXBs under different magnetic braking prescriptions. ApJ **909**, 174 (2021)
30. M. Kilic, P. Bergeron, S. Blouin et al., The most massive white dwarfs in the solar neighbourhood. MNRAS **503**, 5397 (2021)
31. J. Arafune, M. Fukugita, Velocity-dependent factors for the Rubakov process for slowly moving magnetic monopoles. PhRvL **50**, 1901 (1983)
32. A.F. Joshua, F. Katherine, S.T. Michael, Superheavy magnetic monopoles and main-sequence stars. ApJ **335**, 844 (1988)
33. Q.H. Peng, Z.Y. Lie, D.Y. Wang, Content of magnetic monopoles in quasars, galactic nuclei and stars and their astrophysical effects. Scientia Sinica (Serries A) **5**, 466 (1985)
34. C. Super-Kamiokande, K. Ueno, K. Abe, Search for GUT monopoles at Super-Kamiokande. APh **36**, 131 (2012)
35. M.S. Turner, E.N. Parker, T.J. Bogdan, Magnetic monopoles and the survival of galactic magnetic fieldsr. PhRvD **26**, 1296 (1982)
36. E. Parker, The origin of magnetic fields. ApJ **160**, 383 (1970)
37. E. Kolb, M.S. Turner, Limits from the soft X-ray background on the temperature of old neutron stars and on the flux of superheavy magnetic monopoles. ApJ **286**, 702 (1984)
38. J.P. Cox, R.T. Giuli, *Principles of Stellar Structure* (Gordon and Breach, New York, 1968)
39. K. Detlev, C. Ganesar, REVIEW: physics of white dwarf stars. Rep. Prog. Phys. **53**, 837 (1990)
40. S. Ahlen, K. Kinoshita, Calculation of the stopping power of very-low-velocity magnetic monopoles. Phys. Rev. D **26**, 2347 (1982)
41. V. Chandra, H.-C. Hwang, N.L. Zakamska et al., A gravitational redshift measurement of the white dwarf mass–radius relation. ApJ **899**, 146 (2020)
42. J.J. Hermes, W.R. Brown, M. Kilic et al., Radius constraints from high-speed photometry of 20 low-mass white dwarf binaries. ApJ **792**, 39H (2014)
43. S.R.G. Joyce, M.A. Barstow, S.L. Casewell et al., Testing the white dwarf mass–radius relation and comparing optical and far-UV spectroscopic results with Gaia DR2, HST, and FUSE. MNRAS **479**, 1612 (2018)
44. P. Maxted, T. Marsh, P. Wheatley et al., The mass and radius of a low mass white dwarf. In: Spitzer Proposal, p. 60056 (2009)
45. S.G. Parsons, B.T. Gänsicke, T.R. Marsh et al., An accurate mass and radius measurement for an ultracool white dwarf. MNRAS **426**, 1950P (2012)
46. T.-H. Pei, The highly accurate relation between the radius and mass of the white dwarf star from zero to finite temperature. FrASS **8**, 243P (2022)
47. M. Izawa, On stars which burn by the Rubakov process. PThPh **75**, 556 (1986)
48. J. Bartelt, H. Courant, K. Heller et al., New limit on magnetic monopole flux. PhRvL **50**, 655 (1983)
49. A.D. Caplin, C.N. Guy, M. Hardiman et al., New upper bound on the flux of cosmic magnetic monopoles. Nature **317**, 243C (1985)
50. F.C. Adams, M. Fatuzzo, K. Freese et al., Extension of the Parker bound on the flux of magnetic monopoles. PhRvLB **70**, 2511 (1993)
51. L.J. Stone, J.Z. Ajaltouni, R. Becker-Szendy, Magnetic monopole flux limits from catalysis of nucleon decay. ICRC **10**, 87 (1990)
52. R. Becker-Szendy, C.B. Bratton, J. Breault, Magnetic monopole flux limits from the IMB proton decay detector. ICRC **4**, 658 (1993)
53. E.W. Kolb, S.A. Colgate, J.A. Harvey, Monopole catalysis of nucleon decay in neutron stars. PhRvL **49**, 1373 (1982)
54. IceCube Collaboration, R. Abbasi, Y. Abdou, T. Abu-Zayyad et al., Search for relativistic magnetic monopoles with the AMANDA-II neutrino telescope. EPJC **69**, 361 (2010)
55. IceCube Collaboration, M.G. Aartsen, K. Abraham, M. Ackermann et al., Searches for relativistic magnetic monopoles in IceCube. EPJC **76**, 133 (2016)
56. ANTARES Collaboration, A. Albert, M. André, M. Anghinolfi et al., Search for relativistic magnetic monopoles with five years of the ANTARES detector data. JHEP **07**, 054 (2017)
57. D.A. Dicus, D.N. Page, V.L. Teplitz, Two- and three-body contributions to cosmological monopole annihilation. PhRvD **26**, 1306 (1982)
58. B. Joseph, D. Antonio, M. Adam, Multiscatter stellar capture of dark matter. PhRvD **96**, 063002 (2017)
59. D. Basudeb, G. Aritra, R. Anupam, Dark matter capture in celestial objects: improved treatment of multiple scattering and updated constraints from white dwarfs. JCAP **08**, 018D (2019)
60. C. Ilie, S.Y. Zhang, Multiscatter capture of superheavy dark matter by Pop III stars. JCAP **12**, 051 (2019)
61. C. Ilie, C. Levy, Multicomponent multiscatter capture of dark matter. PhRvD **107**, 063003 (2021)
62. N.F. Bell, G. Busoni, M.E. Ramirez-Quezada et al., Improved treatment of dark matter capture in white dwarfs. JCAP **10**, 083B (2021)